AEDC-TDR-64-89

ARCHIVE COPY
DO NOT LOAN

JET INTERFERENCE DURING STAGE SEPARATION AT VERY HIGH ALTITUDES

This document has been approved for public release its distribution is unlimited. Per AF letter dtd 12 Dec, 1975 - William O. Cole -

By

T. W. Binion, Jr.

Propulsion Wind Tunnel Facility

ARO, Inc.

PROPERTY OF U. S. AIR FORCE
AEDC LIBRARY
AF 40(600)1000

TECHNICAL DOCUMENTARY REPORT NO. AEDC-TDR-64-89

May 1964

Program Element 62405334/8953, Task 895301

OFFICIAL USE ONLY

This document may not be released to foreign governments or their representatives without the prior approval of AEDC, Arnold Air Force Station, Tennessee.

(Prepared under Contract No. AF 40(600)-1000 by ARO, Inc., contract operator of AEDC, Arnold Air Force Station, Tenn.)

AEDC TECHNICAL LIBRARY
5 0720 00039 9156

ARNOLD ENGINEERING DEVELOPMENT CENTER

AIR FORCE SYSTEMS COMMAND

UNITED STATES AIR FORCE

NOTICES

Qualified requesters may obtain copies of this report from DDC, Cameron Station, Alexandria, Va. Orders will be expedited if placed through the librarian or other staff member designated to request and receive documents from DDC.

When Government drawings, specifications or other data are used for any purpose other than in connection with a definitely related Government procurement operation, the United States Government thereby incurs no responsibility nor any obligation whatsoever; and the fact that the Government may have formulated, furnished, or in any way supplied the said drawings, specifications, or other data, is not to be regarded by implication or otherwise as in any manner licensing the holder or any other person or corporation, or conveying any rights or permission to manufacture, use, or sell any patented invention that may in any way be related thereto.

~~DDC RELEASE TO OTS IS NOT AUTHORIZED~~

PROPERTY OF U.S. AIR FORCE
AEDC TECHNICAL LIBRARY
ARNOLD AFB, TN 37389

JET INTERFERENCE DURING STAGE SEPARATION AT VERY HIGH ALTITUDES

By

T. W. Binion, Jr.

Propulsion Wind Tunnel Facility

ARO, Inc.

a subsidiary of Sverdrup and Parcel, Inc.

May 1964

ARO Project Nos. PT2000 and PW2112

This document has been approved for public release its distribution is unlimited. Per AF Letter ltr'd 12 Dec, 1975 - William O. Cole -

AF - AEDC
Arnold AFS Tenn

ABSTRACT

Pressure and force measurements were obtained on two upper stage and three lower stage missile models during simulated stage separation. The upper stage rocket engine exhaust was simulated with high pressure carbon dioxide. Data were also obtained at a limited number of test conditions using gaseous nitrogen to simulate the rocket engine exhaust. Data were obtained at ten separation distances with an upper stage nozzle exit pressure ratio variation from 5.5 to 12,914. The test cell pressure ranged from 1.2 to 6300 microns of mercury, which corresponds to an altitude range from 290,000 to 106,000 ft.

The results indicate that interference on the upper stage is dependent on the lower stage configuration and upper stage chamber pressure and is independent of the ambient pressure.

PUBLICATION REVIEW

This report has been reviewed and publication is approved.

Larry R. Walter
1st Lt, USAF
Gas Dynamics Division
DCS/Research

Donald R. Eastman, Jr.
DCS/Research

CONTENTS

	Page
ABSTRACT	iii
NOMENCLATURE	viii
1.0 INTRODUCTION	1
2.0 APPARATUS	
2.1 Test Chambers	1
2.2 Models	2
2.3 Instrumentation	3
3.0 PROCEDURE	
3.1 Cold Wall Vacuum Chamber	4
3.2 18-in. Test Cell	4
4.0 PRECISION OF MEASUREMENTS	5
5.0 RESULTS AND DISCUSSION	
5.1 Tank Dome Pressure Ratio	6
5.2 Interstage Cavity Pressure Distributions	7
5.3 Upper Stage Base Pressure	8
5.4 Lower Stage Drag	9
5.5 Upper Stage Axial Force	10
5.6 Upper Stage Thrust	11
6.0 CONCLUSIONS	11
REFERENCES	12

TABLES

1. Precision of Measurements	13
2. Summary of Test Conditions, Cold Wall Vacuum Chamber	14
3. Summary of Test Conditions, 18-in. Test Cell	17

ILLUSTRATIONS

Figure	
1. Test Chambers	
a. Cold Wall Vacuum Chamber	19
b. 18-in. Test Cell	20

Figure		Page
2.	Test Chamber Installation	
	a. Cold Wall Vacuum Chamber	21
	b. 18-in. Test Cell	22
3.	Model Installation in the Test Chamber	
	a. Cold Wall Vacuum Chamber	23
	b. 18-in. Test Cell	24
4.	Upper Stage Model Configurations	25
5.	Lower Stage Model Configurations	
	a. C_2 Configuration	26
	b. C_{2a} Configuration	27
	c. C_3 Configuration	28
6.	The Effect of Separation Distance and Upper Stage Configuration on Tank Dome Pressure Ratio	
	a. C_2 Configuration	29
	b. C_{2a} Configuration	30
	c. C_3 Configuration	31
7.	Lower Stage Static Pressure Distribution, C_2 Configuration	
	a. $x/d = 0.25$	32
	b. $x/d = 0.50$	33
	c. $x/d = 0.75$	34
	d. $x/d = 1.04$	35
	e. $x/d = 1.50$	36
	f. $x/d = 2.00$	37
8.	Lower Stage Static Pressure Distribution, C_{2a} Configuration	
	a. $x/d = 0$	38
	b. $x/d = 0.25$	38
	c. $x/d = 0.50$	39
	d. $x/d = 1.04$	39
9.	Lower Stage Static Pressure Distribution, C_3 Configuration	
	a. $x/d = 0$	40
	b. $x/d = 0.25$	41
	c. $x/d = 0.75$	42
	d. $x/d = 1.04$	43
	e. $x/d = 1.50$	44
	f. $x/d = 2.00$	45
	g. $x/d = 4.00$	46

Figure		Page
10.	Upper Stage Base Pressure Distribution with C_2 Configuration	
	a. x/d = 0.25	47
	b. x/d = 0.50	47
	c. x/d = 0.75	48
	d. x/d = 1.04	48
	e. x/d = 1.50	48
11.	Upper Stage Base Pressure Distribution with C_{2a} Configuration	
	a. x/d = 0	49
	b. x/d = 0.25	49
	c. x/d = 0.50	49
	d. x/d = 0.75	49
12.	Upper Stage Base Pressure Distribution with C_3 Configuration	
	a. x/d = 0	50
	b. x/d = 0.25	50
	c. x/d = 0.75	51
	d. x/d = 1.04	51
	e. x/d = 1.50	52
	f. x/d = 2.00	52
13.	Effect of Separation Distance and Upper Stage Configuration on Lower Stage Drag	
	a. C_2 Configuration	53
	b. C_{2a} Configuration	54
	c. C_3 Configuration	55
14.	Generalized Lower Stage Drag	56
15.	Effect of Separation Distance on Upper Stage Axial-Force Coefficient	
	a. C_2 Configuration	57
	b. C_{2a} Configuration	58
	c. C_3 Configuration	59
16.	Upper Stage Thrust Coefficient with Each Lower Stage Configuration	
	a. C_2 Configuration	60
	b. C_{2a} Configuration	61
	c. C_3 Configuration	62
17.	Effect of Separation Distance on Axial-Force to Thrust Ratio	63

NOMENCLATURE

A	Area, in.^{2}
A^*	Upper stage nozzle throat area, in.^{2}
a	Velocity of sound, ft/sec
C_a	Upper stage axial-force coefficient, F_a/H_cA_e
C_D	Lower stage drag coefficient, D/MM
C_T	Upper stage thrust coefficient, F_j/H_cA_e
$C_{T_{th}}$	Upper stage theoretical thrust coefficient, $F_{j_{th}}/H_cA_e$
D	Lower stage drag, positive acting downstream, lb
d	Upper stage nozzle exit diameter, 1.25 in.
F_a	Upper stage axial force, positive acting upstream, lb
F_j	Upper stage thrust, $F_a - A_b(0.2p_{14} + 0.3p_{15} + 0.5p_{23})$, lb
$F_{j_{th}}$	Upper stage theoretical vacuum thrust, $H_cA_e\left[\frac{p_e}{H_c} + \left(\frac{\rho_e}{\rho_c}\right)\left(\frac{\rho_c}{H_c}\right)(M_e a_e)^2\right]\left[1/2\,(1 + \cos\theta_N)\right]$, lb
H_c	Upper stage nozzle total pressure, psi or psf
M	Mach number
MM	Jet momentum, $\gamma_c\left(\frac{p_e}{H_c}\right)H_c\,M_e^2\,A_e$, lb
M_y	Mach number behind normal shock at nozzle exit
p	Pressure, psi or microns of mercury
p_{ty}	Total pressure behind normal shock at nozzle exit, psi
R	Upper stage model radius, in., or perfect gas constant, ft-lb$_f$/slug-°R
r	Radius, in.
T	Temperature, °R
x	Stage separation distance, in. (see Fig. 5)
x'	Distance from upper stage base to most forward portion of lower stage, in. (see Fig. 4)

Z	Compressibility factor
γ	Specific heat ratio
θ_N	Nozzle half angle, deg
ρ	Density, slugs/ft^3
ρ_c	Density of the carbon dioxide in rocket chamber, H_c/Z_cRT_c, slugs/ft^3
ϕ	Lower stage diameter, in.

SUBSCRIPTS

b	Upper stage base
c	Upper stage rocket chamber
e	Upper stage nozzle exit
1 through 8	Lower stage pressure orifices (see Fig. 5)
9	Orifice at center of lower stage tank dome
14, 15, 23	Upper stage pressure orifices
∞	Ambient conditions

CONFIGURATIONS

C_2	Two-inch-diameter lower stage (Fig. 5a)
C_{2a}	Two-inch-diameter lower stage with interstage fairing removed (Fig. 5b)
C_3	Three-inch-diameter lower stage (Fig. 5c)
N_1	Upper stage with $A_e/A^* = 8.33$ nozzle (Fig. 4)
N_2	Upper stage with $A_e/A^* = 15.5$ nozzle (Fig. 4)

1.0 INTRODUCTION

One of the critical operations during a missile flight concerns stage separation. If the upper stage ignition occurs too soon after separation, interference with the lower stage can adversely affect the operation and performance of the upper stage. A long interval between stage separation and upper stage ignition results in an extended coast time, which could also adversely affect missile performance. A knowledge of the pressures, forces, and flow field about the two stages during separation could lead to an optimum coast time for the staging operation.

The investigation reported herein is an extension of that reported in Ref. 1 to include two additional lower stage configurations, a larger area ratio upper stage nozzle, and another nozzle fluid. Data were also obtained with the configuration in Ref. 1 but at smaller ($x/d < 1$) separation distances. The tests were conducted under the sponsorship of the Arnold Engineering Development Center (AEDC), Air Force Systems Command (AFSC), in the PWT Cold Wall Vacuum Chamber and an 18-in. Test Cell. Most of the test data were obtained with carbon dioxide as the upper stage nozzle fluid. An isentropic expansion of CO_2 from the total pressure of the rocket chamber to the low ambient pressure of the vacuum chamber may induce condensation of the CO_2 in parts of the jet plume. Therefore, data were obtained in an 18-in. Test Cell employing nitrogen as the nozzle fluid to evaluate the effect of the possible condensation of CO_2 on the measured parameters.

Altitude pressure in the test chambers is a function of several operating parameters and therefore was a dependent variable. However, an effective altitude variation was accomplished through the parameter $\frac{\text{nozzle exit pressure}}{\text{altitude pressure}}$ by variation in the nozzle total pressure. Data were obtained with two upper stage nozzle configurations and three lower stage configurations at stage separation distances from zero to 8 nozzle exit diameters with a rocket chamber pressure variation from 20 to 100 psi. The nozzle exit pressure ratio variation was from 5.5 to 12,914.

2.0 APPARATUS

2.1 TEST CHAMBERS

2.1.1 PWT Cold Wall Vacuum Chamber

The Propulsion Wind Tunnel (PWT) Cold Wall Vacuum Chamber (Fig. 1a) was designed to allow testing at altitudes of 100,000 to

---

Manuscript received April 1964.

300,000 ft with cold surfaces being utilized to cryopump a simulated rocket exhaust. Carbon dioxide was selected as the nozzle fluid because it can be readily cryopumped at liquid nitrogen temperatures. The CO_2 was superheated to about 600°F to delay condensation, in the jet, as it expanded to the altitude pressure. However, because of heat losses in the CO_2 piping and the Joules-Thompson expansion across the pressure control valve, the total temperature is reduced to about 425°F in the rocket chamber. A complete description of the Cold Wall Vacuum Chamber and its operating characteristics is presented in Ref. 2. The vacuum chamber installation is shown in Fig. 2a, and the installation of the N_1C_3 model configuration is shown in Fig. 3a.

2.1.2 18-in. Test Cell

The 18-in. Test Cell (Fig. 1b) was designed to use the six-stage steam ejector system of the PWT Lorho 18-in. Wind Tunnel to pump the gaseous nitrogen. It consists of a circular duct 18 in. in diameter and 30-in. long flanged to the steam ejector system. The test cell installation is shown in Fig. 2b, and the N_1C_2 configuration installation is shown in Fig. 3b.

2.2 MODELS

2.2.1 Upper Stage

The basic dimensions of the upper stage models and the pressure orifice locations are presented in Fig. 4. The upper stage models differed only in throat diameter and fabrication tolerances. The thermodynamic properties of carbon dioxide at the nozzle exit were calculated by assuming a thermodynamic equilibrium isentropic expansion from stagnation conditions. The values for the carbon dioxide properties were obtained from the Mollier diagram for carbon dioxide in Ref. 3. The normal shock values were obtained by calculating the intersection of the Fanno and Rayleigh lines from the nozzle exit conditions. The stagnation conditions with CO_2 for the calculations of the exit parameters presented below were assumed to be 482°F and 50 psi. The deviation in the actual stagnation conditions from those assumed would change the nondimensional exit parameters, with the exception of ρ_e/ρ_c, by less than four percent because of the deviation of the properties of CO_2 from the perfect gas concept. The deviation of ρ_e/ρ_c is less than 9 percent. The flow parameters for nitrogen at the nozzle exit were calculated from isentropic perfect gas equations since the real gas effects with nitrogen are insignificant in the operating range of this investigation. The pertinent exit parameters are presented in the table on the following page.

Nozzle	Fluid	A_e/A^*	θ_N, deg	M_e	p_e/H_c	p_{ty}/H_c	M_y
N_1	CO_2	8.33	18.2	3.29	0.0130	0.160	0.442
N_1	Nitrogen	8.33	18.2	3.72	0.0096	0.175	0.443
N_2	CO_2	15.50	17.4	3.85	0.0054	0.086	0.436

Nozzle	Fluid	ρ_e/ρ_c	T_e/T_c	a_e, ft/sec	γ_c	γ_e
N_1	CO_2	0.0335	0.390	761	1.227	1.34
N_1	Nitrogen	0.0363	0.363	775	1.398	1.40
N_2	CO_2	0.0175	0.305	666	1.227	1.40

2.2.2 Lower Stage

The basic dimensions of the lower stage configurations and pressure orifice locations are presented in Fig. 5. The tank dome is a spherical segment with a radius equal to the interstage inside diameter. The thickness of the interstage fairing could not be scaled because of strength requirements; however, the outer surface of the fairing was tapered to reduce its thickness as much as possible. The C_{2a} model was obtained by removing the interstage fairing from the C_2 model.

2.3 INSTRUMENTATION

Model instrumentation consisted of five pressure orifices on the upper stage model and nine on the lower stage model, as shown in Figs. 4 and 5. The 14 model pressures were measured by electromechanical transducers. The upper stage axial force was measured by strain gages located on the nozzle fluid supply piping, as indicated in Fig. 4. The lower stage axial force was measured with a three-component internal balance indicated in Fig. 5.

The pressures at the upstream and downstream ends of the Cold Wall Vacuum Chamber were measured by two Alphatrons connected to the pressure orifices shown in Fig. 1a. The upstream orifice was located in the center of the chamber behind the model support structure, and the measurement at this orifice was considered to be the altitude pressure. The reading of the Alphatron is a function of gas composition at a given pressure. Therefore, each reading obtained in the Cold Wall Vacuum Chamber was multiplied by the manufacturer's correction factor of

0.633 for carbon dioxide. The altitude pressure in the 18-in. Test Cell was also measured at an orifice upstream of the model (Fig. 1b) by an Alphatron. The Alphatron readings obtained in the 18-in. Test Cell did not require a gas composition correction.

3.0 PROCEDURE

3.1 COLD WALL VACUUM CHAMBER

The day before testing, the carbon dioxide conditioning vessel was filled with approximately 300 lb of carbon dioxide, and superheating was begun. Approximately six hours were required to heat the carbon dioxide to 600°F. A thermostat control device was then employed to maintain the desired temperature. Pumpdown of the vacuum chamber required about ten minutes; however, the chamber was kept in an evacuated condition whenever possible.

Chilldown of the vacuum chamber was begun about 1.5 hours before test time. Upon completion of chilldown and immediately preceding the start of carbon dioxide flow, the liquid nitrogen flow rate was increased to between 50 and 120 gpm, depending on the desired carbon dioxide flow rate. The "firing" was accomplished by opening two shutoff valves (Ref. 2) and manually loading a pneumatic throttling valve. Data recording was begun as soon as the chamber pressure became stable at the desired value. The average time required for a data point was about 1.5 minutes. The "firing" was terminated by closing the throttle valve. Data were obtained at an average of three chamber pressure settings at each separation distance. The separation distance was varied by a rack and pinion traversing mechanism from outside the vacuum chamber. The separation distance was measured from the upper stage base to the leading edge of the interstage fairing (Fig. 4). The separation distance for the C_{2a} configuration was measured as if the interstage fairing were still in place so that the distance from the upper stage base to the tank dome at a given x/d was the same for each configuration.

When testing was completed, the chamber was allowed to warm to ambient temperature while the condensed carbon dioxide sublimated. Mechanical pumping was continued to remove the carbon dioxide gas.

3.2 18-IN. TEST CELL

After the 18-in. Test Cell had been evacuated by the six-stage steam ejector system, the desired nitrogen flow rate was established to the

model by a suitable system of valves and pressure regulators. The nitrogen was heated to 400°F by a controllable resistance heating element contained in the supply piping. Data were recorded after steady-state conditions had been obtained. The separation distance was manually adjusted and measured in the same manner defined in paragraph 3.1.

4.0 PRECISION OF MEASUREMENTS

An estimate of the precision of the measurements is presented in Table 1. The Alphatrons which were used to obtain the vacuum chamber pressure were calibrated with air versus a McLeod gage in a cold-trapped calibration system. The Alphatron reading is a function of the composition of the gas in the ionization chamber. The gas composition at the measuring orifice in the Cold Wall Vacuum Chamber was a mixture of air and carbon dioxide. The quantitative composition of the gas in the Alphatron is not known. However, since the vacuum chamber atmosphere during a data point was primarily carbon dioxide, the manufacturer's correction of 0.633 for carbon dioxide was applied to the data. The gas composition in the 18-in. Test Cell was nitrogen-rich air; therefore, no correction of the Alphatron reading was required. The accuracy listed in Table 1 for p_∞ applies to the Alphatron and does not include any error caused by the gas composition uncertainty.

The model pressure accuracies were estimated from transducer calibration data and include non-linearity and hysteresis effects. The upper stage force measurement was sensitive to the temperature of the piping. Therefore, a datum reading was taken without nozzle flow immediately following each data point to eliminate the temperature uncertainty.

5.0 RESULTS AND DISCUSSION

Data were obtained at ten stage separation distances from $x/d = 0$ to 8 with the upper stage rocket chamber pressure varied in five steps from 20 to 100 psi. The pressure in the upstream portion of the test chambers, p_∞, was dependent on the model configuration, model position, rocket chamber pressure, and also on solid carbon dioxide buildup in the Cold Wall Vacuum Chamber. It was therefore impossible to use p_∞ as an independent variable. Altitude variation was accomplished through the nozzle exit pressure ratio, p_e/p_∞. It should be recognized that p_e/p_∞, while indicative of jet spreading and an effective parameter for altitude simulation, has doubtful meaning when the upper stage nozzle is within

the interstage fairing. The interaction of the two stages caused considerable flow into the upstream portion of the test chamber in some instances. The measurement of the altitude pressure in these instances would reflect some component of the reverse flow total pressure because of the probe location. The actual pressure to which the flow expanded was probably lower than indicated. However, as shown in Ref. 1, the measured parameters for the lower stage model were independent of the ambient pressure within the range of this investigation. A summary of test conditions presented in Tables 2 and 3 shows an altitude pressure range from 1.3 to 6300 microns of mercury, which corresponds to an altitude range from 290,000 to 106,000 ft.

5.1 TANK DOME PRESSURE RATIO

The variation of the pressure ratio at the center of the tank dome with separation distance x/d for each configuration is presented in Fig. 6. The tank dome pressure ratio would be influenced by that portion of the upper stage nozzle which is within the interstage cavity, since the nozzle external configuration in conjunction with the interstage fairing determines the area available for the flow to escape to the surroundings. However, the upper stage external configuration was not varied in this investigation. The change in the nozzle area ratio apparently does not affect the basic shock structure within the interstage cavity (or external to the lower stage at $x/d > 1.04$) but does affect the magnitude of the phenomena, as indicated by comparing the N_1 and N_2 data for each lower stage configuration. The nozzle area ratio influences the magnitude of the pressures on the lower stage because, at a given distance downstream of the nozzle exit, the Mach number of the jet will be greater with the N_2 nozzle than the N_1 nozzle. Since the flow from the nozzle is supersonic, some type of shock system must be present in front of the tank dome. The shock system would therefore occur at a higher Mach number with the N_2 nozzle, resulting in a higher total pressure loss through the shock system than would be obtained with the N_1 nozzle.

The total pressure recovery for a normal shock at the nozzle exit is indicated in Fig. 6a and corresponds to the tank dome pressure ratio at $x/d = 0.5$. If the nozzle flow were separated, the shock system within the nozzle would occur at a Mach number lower than the nozzle exit Mach number for fully expanded flow; hence, the recovery would be higher than the exit normal shock recovery as reflected in the tank dome pressure ratio at $x/d = 0.25$. The tank dome pressure ratio obtained with nitrogen at $x/d = 0.25$ and 0.50 are slightly higher than those obtained with CO_2, as would be expected since p_{ty}/H_c is higher for nitrogen than for CO_2.

The high pressure ratio between x/d = 0.75 and 1.04 must be due to the shock structure within the interstage cavity. The shock structure is probably the same with the three sets of data. The pressure ratios with nitrogen are greater than those with CO_2 because the combination of Mach number and specific heat ratio before the shock system with nitrogen results in a higher total pressure recovery across the shock system. The data fairing was omitted between x/d = 0.75 and 1.04 because the peak pressure in that region was not defined. As the separation distance increases beyond x/d = 1.04 (the interstage cavity beyond the nozzle exit), the Mach number of the jet flow field in front of the lower stage increases. The tank dome pressure ratio therefore decreases with increasing separation distance because of the increasing shock and mixing losses at the higher Mach numbers.

Removal of the interstage fairing (C_{2a} configuration) greatly reduces the tank dome pressure ratio at each separation distance, as may be seen by comparison of Figs. 6a and b. Removal of the interstage fairing also results in a monotonic variation of the tank dome pressure ratio with separation distance. The tank dome pressure ratios obtained with the C_3 configuration (Fig. 6c) are equivalent to those of the C_{2a} configuration up to a separation distance of x/d = 1.04. The difference in the tank dome pressure ratio between the C_{2a} and C_3 configurations and the C_2 configuration from x/d = 0 to 1.04 may be attributed to the larger "escape area" between the nozzle and the interstage fairing with the C_{2a} and C_3 configurations, thereby creating a different shock structure within the interstage cavity than was obtained with the C_2 configuration.

5.2 INTERSTAGE CAVITY PRESSURE DISTRIBUTIONS

The pressure distributions within the interstage cavity are shown in Figs. 7 through 9 for the three lower stage configurations. The pressure distribution at x/d = 0.25 and 0.5 for the C_2 configuration (Figs. 7a and b) indicates a reasonably constant pressure region at the tank dome. Also, the distribution indicates possible model misalignment or unsymmetrical flow separation. However, the data from the two test chambers produce essentially identical tank dome pressure distributions, which tends to rule out model misalignment producing an unsymmetrical distribution. From geometrical considerations, the velocity vector within the interstage fairing must be toward the upper stage. The pressure ratios at orifices 1 and 2 are higher than at 3 and 4, which indicates a decelerating flow toward the upper stage. The minimum geometrical area for the flow toward the surroundings at x/d greater than 0.2 is between the interstage fairing and the nozzle rather than between the interstage fairing lip and the upper stage base.

The pressure distributions at x/d = 0.75 and 1.04 (Figs. 7c and d) show a strong pressure gradient on the tank dome. The velocity along the interstage fairing is apparently constant, as indicated by the pressure ratio at orifices 1 through 4. The pressure gradients across the tank dome are diminished at x/d = 1.5, as indicated in Fig. 7e. The data obtained with nitrogen suggest a slightly stronger back flow, indicated by the lower pressures at orifices 1 and 2. The stronger back flow results from the inability to obtain nozzle pressure ratios, p_e/p_∞, in the 18-in. Test Cell sufficient to expand the jet to a diameter much greater than the lower stage diameter. At large separation distances, a shock system is present in front of the lower stage, and the fluid within the interstage cavity is stagnant. The lower stage acts as a blunt body, and the pressure ratio within the interstage cavity is practically uniform, as shown at x/d = 2 in Fig. 7f. The distribution at x/d = 2 is typical of all separation distances greater than x/d = 2.0 for the C_2 configuration.

Removal of the interstage fairing results in the pressure distributions shown in Fig. 8. The large pressure gradients at x/d = 0 (Fig. 8a) are probably due to the large radial Mach number gradient (the Mach number increases as the radial distance from the jet centerline increases) in the flow approaching the tank dome. As the separation distance increases, the radial Mach number gradient decreases, resulting in a more uniform flow field in the region of the tank dome. Hence, the tank dome pressure gradient decreases with increasing separation distance as indicated in Fig. 8.

The pressure distribution within the interstage cavity of the C_3 configuration is presented in Fig. 9. As the separation distance increases from zero to 1.04, the pressure gradient across the tank dome diminishes. At x/d = 1.5, the pressure distribution is very flat across the tank dome and is similar to that obtained with the C_2 configuration at x/d = 0.25 and 0.50 (Figs. 7a and b). The pressure distribution along the interstage fairing indicates an accelerating velocity component in the upstream direction at separation distances as far as x/d = 2, whereas there was no indication of reverse flow with the C_2 configuration beyond x/d = 1.5. The pressure distribution at x/d = 4 is typical of greater separation distances.

5.3 UPPER STAGE BASE PRESSURE

The base pressure distribution on the upper stage with the C_2 configuration (Fig. 10) indicates impingement of the reverse flow from the nozzle from x/d = 0.25 to 1.5. The base pressure at x/d greater than 2

was less than 0.005 psi (lower limit of transducer). As with the lower stage, the N_2 nozzle results in a distribution which is very similar to that of the N_1 nozzle but lower in magnitude. The base pressure ratio for each nozzle decreases with increasing x/d as would be expected. The base pressure ratios obtained with nitrogen are the same as obtained with CO_2 except at x/d = 1.5, where the nozzle pressure ratio was too low to expand the jet to a diameter much greater than the lower stage diameter.

The upper stage base pressure ratios obtained with the C_{2a} configuration (Fig. 11) are lower by more than a factor of ten (at a given x/d) than those obtained with the C_2 configuration, as may be seen by comparing Figs. 10 and 11. The base pressures at x/d greater than 1.04 for the N_1 and x/d greater than 0.5 for the N_2 nozzle were less than 0.005 psi. The base pressure distribution resulting from the interference of the C_{2a} lower stage is also considerably different than that for the C_2 configuration (Fig. 10), indicating that the reverse flow pattern is not the same with the two configurations. This is to be expected since the flow restraining action of the interstage fairing is not present.

The base pressure distribution produced with the C_3 configuration shown in Fig. 12 indicates still another flow pattern associated with the reverse flow at x/d = 0 and 0.25. However, the pressure level is about a factor of five lower than with the C_2 configuration. At separation distances beyond x/d = 0.75, the pressure distribution is very similar to that produced with the C_2 configuration (Fig. 10). The reverse flow impingement on the upper stage persists as far as x/d = 2 with the C_3 configuration, as was indicated by the interstage cavity pressure distribution (Fig. 9). Base pressures with the C_3 configuration at x/d = 4 were below the sensitivity of the transducers.

5.4 LOWER STAGE DRAG

The lower stage drag coefficient for the three configurations is presented in Fig. 13. The ratio of the lower stage drag to the jet exit momentum is an effective parameter for comparison of the data obtained with the two nozzles and two nozzle fluids. A complete elastic reversal of the jet within the interstage cavity would yield $C_D = 2.0$. The fact that C_D exceeds 2.0 at the low values of x/d with the C_2 and C_3 configurations indicates that a phenomenon other than an elastic reversal of the jet occurs when the interstage fairings are present.

The drag coefficient for the C_2 configuration (Fig. 13a) does not show the effect of the high pressure at the center of tank dome at x/d = 0.75 and 1.04 as indicated in Figs. 7c and d. Apparently, the high pressure

at the tank dome center is a localized condition and does not make a significant contribution to the total drag force.

Removal of the interstage fairing resulted in a constant drag coefficient to $x/d = 0.25$ (Fig. 13b). At separation distances beyond $x/d = 0.25$, the drag coefficient decreases because of the decrease in the percentage of the total jet flow intercepting the lower stage. The lower value of the C_{2a} drag coefficient, as compared to the C_2 drag coefficient, is due to the definition of the separation distance. If a separation distance x' is employed as shown in Fig. 4, the values of the drag coefficient for the C_2 and C_{2a} configurations are in reasonable agreement from $x/d = 1.2$ to 8. This further substantiates the conclusion from the interstage cavity pressure distribution of the C_2 configuration (Fig. 7) that the lower stage acts as a blunt body after the upper stage nozzle exit moves beyond the interstage fairing. The drag coefficient of the C_3 configuration is presented in Fig. 13c. The drag coefficient is in general higher than for the smaller lower stage configuration at a given x/d, because a larger percentage of the jet is intercepted by the C_3 configuration.

If the separation parameter x'/ϕ is used rather than x/d, the lower stage drag coefficient C_D for the three lower stage configurations may be reduced to a single band of data as shown in Fig. 14. It should be noted that two configuration parameters were held constant in this investigation: the upper stage nozzle exit diameter and the lower stage tank dome configuration. It is improbable that the upper stage nozzle exit diameter would affect the lower stage drag coefficient, provided the expanded jet diameter was at least between 1 and 2 times the lower stage diameter. The lower stage tank dome configuration could affect the shock structure and recirculating gas velocities at small separation distances ($x/d < 1$), thereby affecting the drag parameter.

5.5 UPPER STAGE AXIAL FORCE

The upper stage axial-force coefficient with the C_2 configuration (Fig. 15a) decreases as x/d increases to a value comparable to theoretical vacuum thrust at x/d greater than 2.0. The data obtained with nitrogen agrees reasonably well with the data obtained with CO_2 except at $x/d = 1.5$, which is due to an increase in the base pressure discussed in paragraph 5.3. The agreement between theory and the arithmetic average of all interference-free (base pressure less than 0.005 psi) experimental upper stage force data is 4.5 and 3.5 percent for the N_1 and N_2 nozzles, respectively. The axial-force coefficient at $x/d = 0.25$,

C_2 configuration, is almost twice that at an interference-free condition, whereas with the interstage fairing removed (C_{2a}) (Fig. 15b), the axial-force coefficient at $x/d = 0.25$ is only about ten percent higher than the interference-free condition. Further, no interference is indicated beyond $x/d = 1.0$. Removal of the interstage fairing greatly reduced the interference effects on the upper stage. The interference could possibly be reduced more by changing the tank dome design. With proper tank dome design and interstage venting, it seems probable that upper stage ignition could occur at zero separation distance. The C_3 configuration produces interference reflected in the axial-force coefficient (Fig. 15c) as far as $x/d = 2.0$. However, the maximum magnitude of the axial-force coefficient is only about 39 percent above interference-free conditions, as compared with 100 percent for the C_2 configuration.

5.6 UPPER STAGE THRUST

The increase in the upper stage axial force at low separation distances is due to flow impingement on the base. The upper stage axial-force coefficient was corrected for the base pressure, and the thrust coefficient thus obtained is presented in Fig. 16. The agreement between the thrust coefficient obtained with nitrogen and CO_2 is very good, as shown in Fig. 16a. Since the measured thrust agrees with the theoretical thrust, it could be concluded that the nozzle flow is not separated. However, it should be noted that the decrease in thrust which would result from a completely separated nozzle flow is within the scatter of the data.

The contribution of the base pressure to upper stage axial force is clearly indicated by the ratio of axial-force coefficient to thrust coefficient, C_a/C_t, as presented in Fig. 17. The values of C_a/C_t greater than unity are the result of recirculating jet exhaust gases impinging on the upper stage base. The data are presented versus the separation parameter x'/ϕ to indicate that the interference of each lower stage configuration ceases at the same value of x'/ϕ.

6.0 CONCLUSIONS

Pressures and forces were obtained on two upper stage model configurations with three lower stage configurations at separation distances from $x/d = 0$ to 8 and nozzle exit pressure ratios, p_e/p_∞, from 5.5 to 12,914. The results indicate the following conclusions:

1. The interference on the upper stage is dependent on the lower stage configuration.

2. For a given upper and lower stage configuration, the interference on the upper stage was reduced by employing a larger area ratio upper stage nozzle.

3. Removal of the interstage fairing reduces the upper stage interference.

4. The pressure ratio on the lower stage tank dome is reduced by removal of the interstage fairing.

5. Although increasing the size of the lower stage with respect to the upper stage (C_3 configuration) results in less maximum interference, the interference effects are present at greater separation distances.

6. For a given two-stage configuration, the interstage cavity pressure ratio (p/H_c) distribution and the drag coefficient of the lower stage are a function of separation distance.

7. The variation in nozzle fluid at the test conditions where comparison could be made had no effect on the measured parameters.

REFERENCES

1. Binion, T. W., Jr. and Herron R. D. "Pressures and Forces on a Missile Model Resulting from Stage Separation at Very High Altitudes." AEDC-TDR-62-195, November 1962.

2. Herron, R. D. and Binion, T. W., Jr. "The Application of Cryogenic Pumping in a High Mass Flow System." AEDC-TDR-63-199, October 1963.

3. ASHRAE Guide and Data Book, American Society of Heating, Refrigeration and Air-Conditioning Engineering, Inc., 1961.

TABLE 1

PRECISION OF MEASUREMENTS

Vacuum chamber pressure, p_∞	±2 percent
Nozzle total pressure, H_c	±0.1 psi
Lower stage model pressure, p_1 through p_9	±0.06 psi
Upper stage model pressure, p_{14}, p_{15}, p_{23}	±0.005 psi
Upper stage axial force, F_a	±1 percent
Lower stage drag, D	±1 percent

TABLE 2

SUMMARY OF TEST CONDITIONS, COLD WALL VACUUM CHAMBER

x/d	H_c, psi	p_∞, μ of Hg	p_e/p_∞	x/d	H_c, psi	p_∞, μ of Hg	p_e/p_∞
N_1C_2 CONFIGURATION							
4	19.9	19	706	1.00	20.1	58	232
	19.9	51	264		66.9	823	5.5
	20.1	8.2	1651	0.75	20.1	30	441
	30.6	13	1612		20.1	51	266
	51.5	39	881		30.0	53	380
	49.9	34	662		66.9	38	1185
	67.2	51	891		67.1	823	5.5
	99.6	127	529	0.50	19.9	29	460
2	20.1	29	468		20.1	39	344
	67.2	25	1793		30.0	58	346
1.5	20.4	51	270		66.9	418	107
	67.2	63	71		67.1	823	5.5
1.04	19.9	63	212	0.25	19.9	23	569
	20.1	51	266		30.0	56	362
	30.0	126	159		49.9	234	143
	67.3	6330	7		49.9	316	106
N_2C_2 CONFIGURATION							
4.1	30.1	5.7	1,401	0.75	21.0	19	286
	65.4	1.3	12,916		30.5	29	270
	100.0	15	1,718		66.0	190	90
2.0	30.5	27	297	0.50	20.1	14	369
	65.8	82	132		30.7	25	324
1.5	31.2	49	163		66.0	108	158
	66.5	101	170	0.25	20.4	12	435
1.04	20.7	41	130		30.5	16	501
	29.4	32	239		65.7	76	223
	65.5	127	134				

TABLE 2 (Continued)

x/d	H_c, psi	p_∞, μ of Hg	p_e/p_∞	x/d	H_c, psi	p_∞, μ of Hg	p_e/p_∞
N_1C_{2a} CONFIGURATION							
8	67.9	4.4	9969	0.75	19.9	52	258
4	69.9	13	3684		31.0	101	206
3	68.1	29	1572		66.0	443	100
2	20.5	7	2010	0.50	50.1	380	89
	67.2	76	595	0.25	30.0	146	138
1.5	20.5	16	86		51.8	506	69
	67.0	120	375	0	30.3	165	123
1.04	20.4	34	403		30.0	190	106
	30.0	70	289				
	67.0	247	183				
N_2C_{2a} CONFIGURATION							
4	67.0	41	4,072	0.50	20.4	13	403
2	32.4	7.6	1,113		31.5	30	267
	67.0	25	706		67.4	114	153
1.5	31.5	11	754	0.25	67.0	171	101
	67.5	32	550	0	30.0	25	311
1.04	20.8	12	445		50.2	76	171
	30.9	18	436		99.9	418	617
	67.2	76	229				

TABLE 2 (Concluded)

x/d	H_c, psi	p_∞, μ of Hg	p_e/p_∞	x/d	H_c, psi	p_∞, μ of Hg	p_e/p_∞
N_1C_3 CONFIGURATION							
7.5	67.5	3.4	12,604	0.75	20.8	42	335
4	67.2	32	1,423		30.3	139	146
2	20.7	25	552		67.2	696	65
	67.5	53	85	0.50	30.0	190	106
1.5	20.4	39	349	0.25	30.3	241	85
	67.5	1,076	42		49.8	570	59
1.04	20.2	34	408	0	30.1	247	82
	30.3	120	169		50.9	570	12
	67.2	886	51				
N_2C_3 CONFIGURATION							
7.5	67.9	29	603	1.04	31.0	25	318
	67.8	23	744		67.6	89	197
4	67.6	18	972	0.75	30.6	21	378
2	21.2	29	187		67.6	108	162
	67.5	70	250	0.50	30.6	19	416
1.5	20.1	22	234	0.25	30.0	16	484
	30.6	57	138		50.7	63	207
	67.5	76	230	0	30.6	15	510
					50.2	89	146

TABLE 3

SUMMARY OF TEST CONDITIONS, 18-IN. TEST CELL

N_1C_2 CONFIGURATION

x/d	H_c, psi	p_∞, μ of Hg	p_e/p_∞
1.5	17.9	1000	8.9
1.5	24.0	1400	8.5
1.5	30.1	1700	8.8
1.04	30.0	1450	10.3
0.75	17.8	940	9.4
0.75	30.1	1540	9.7
0.50	18.1	909	9.9
0.50	28.0	1300	10.7
0.25	17.9	760	11.7
0.25	23.9	1000	11.4

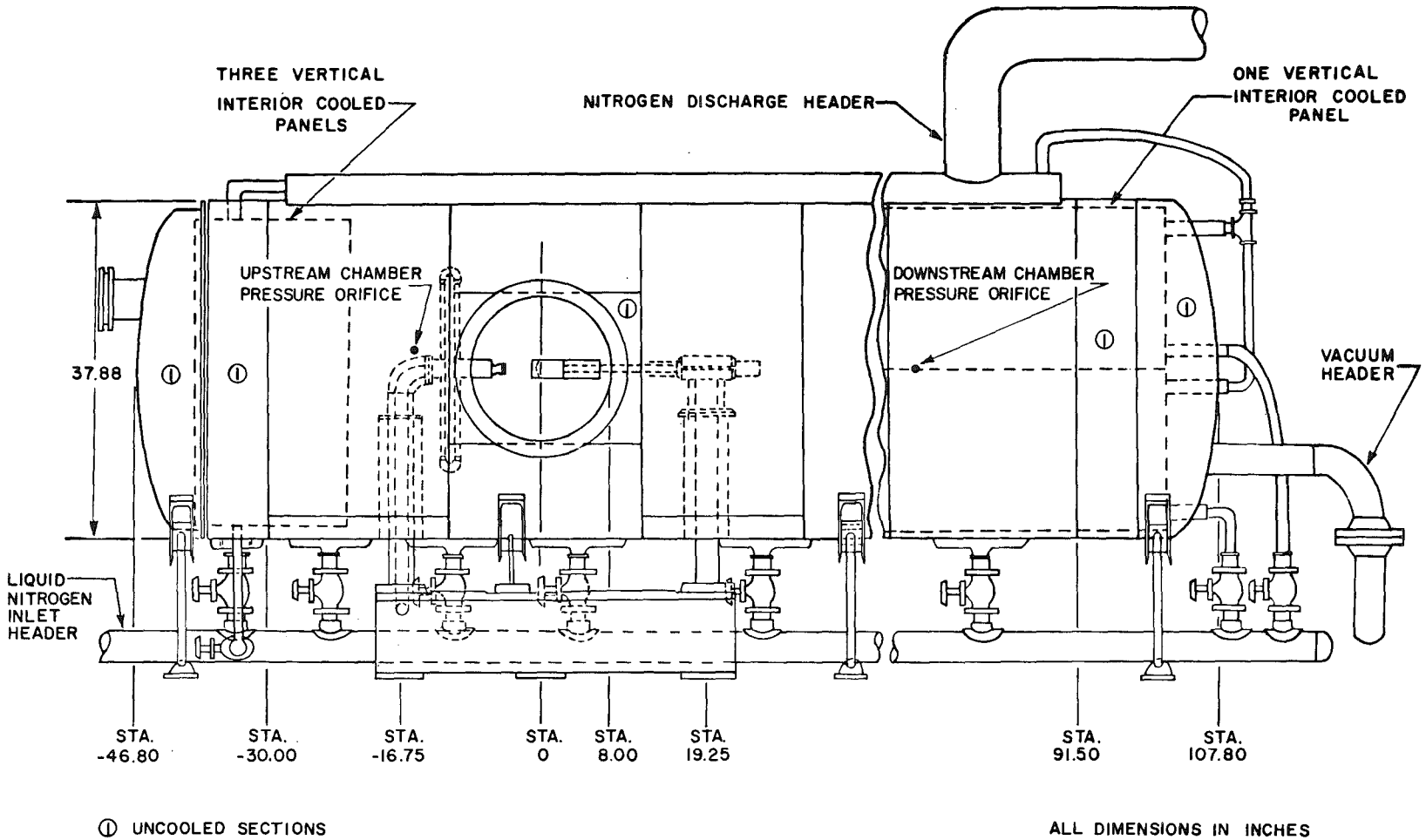

a. Cold Wall Vacuum Chamber

Fig. 1 Test Chambers

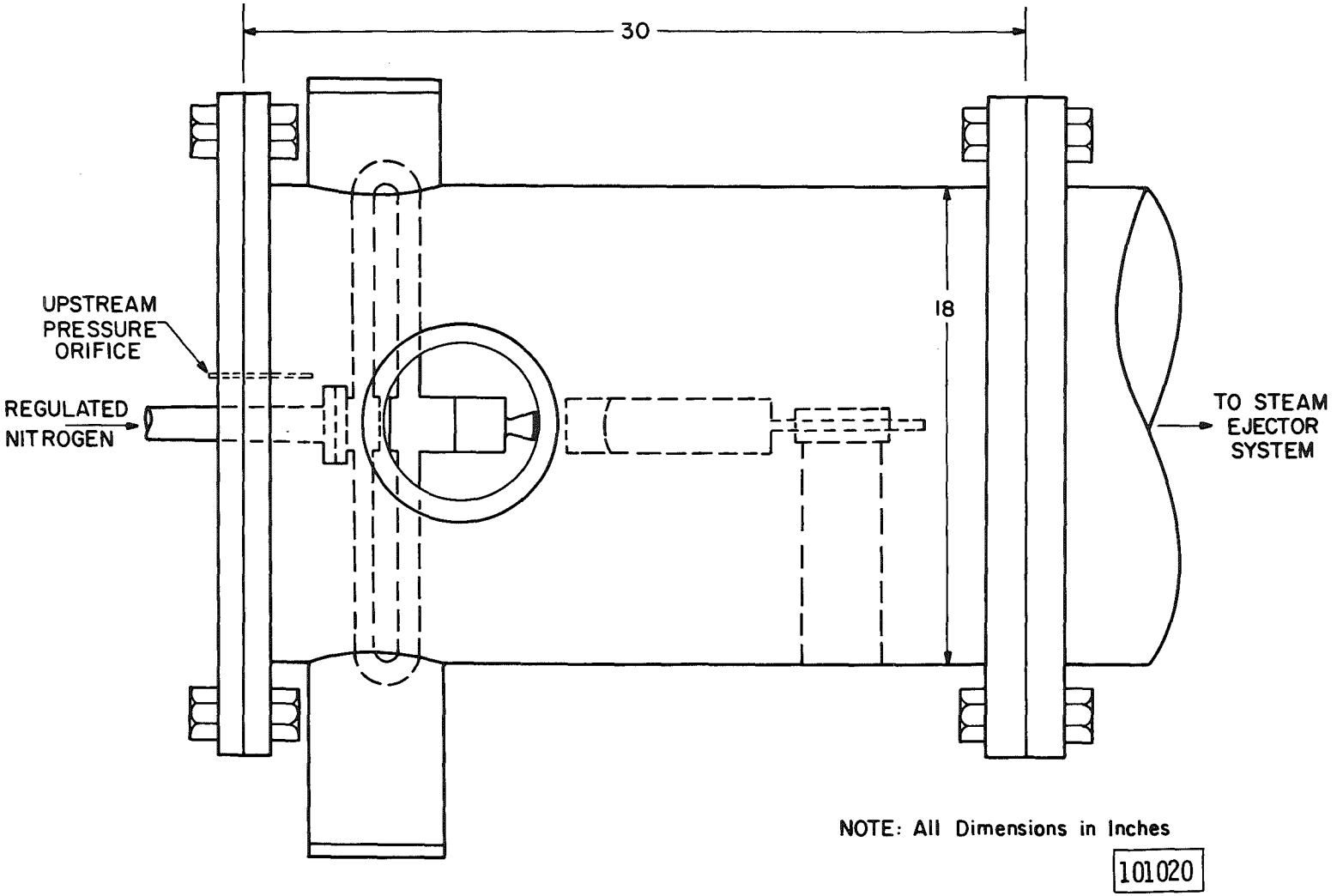

b. 18-in. Test Cell

Fig. 1 Concluded

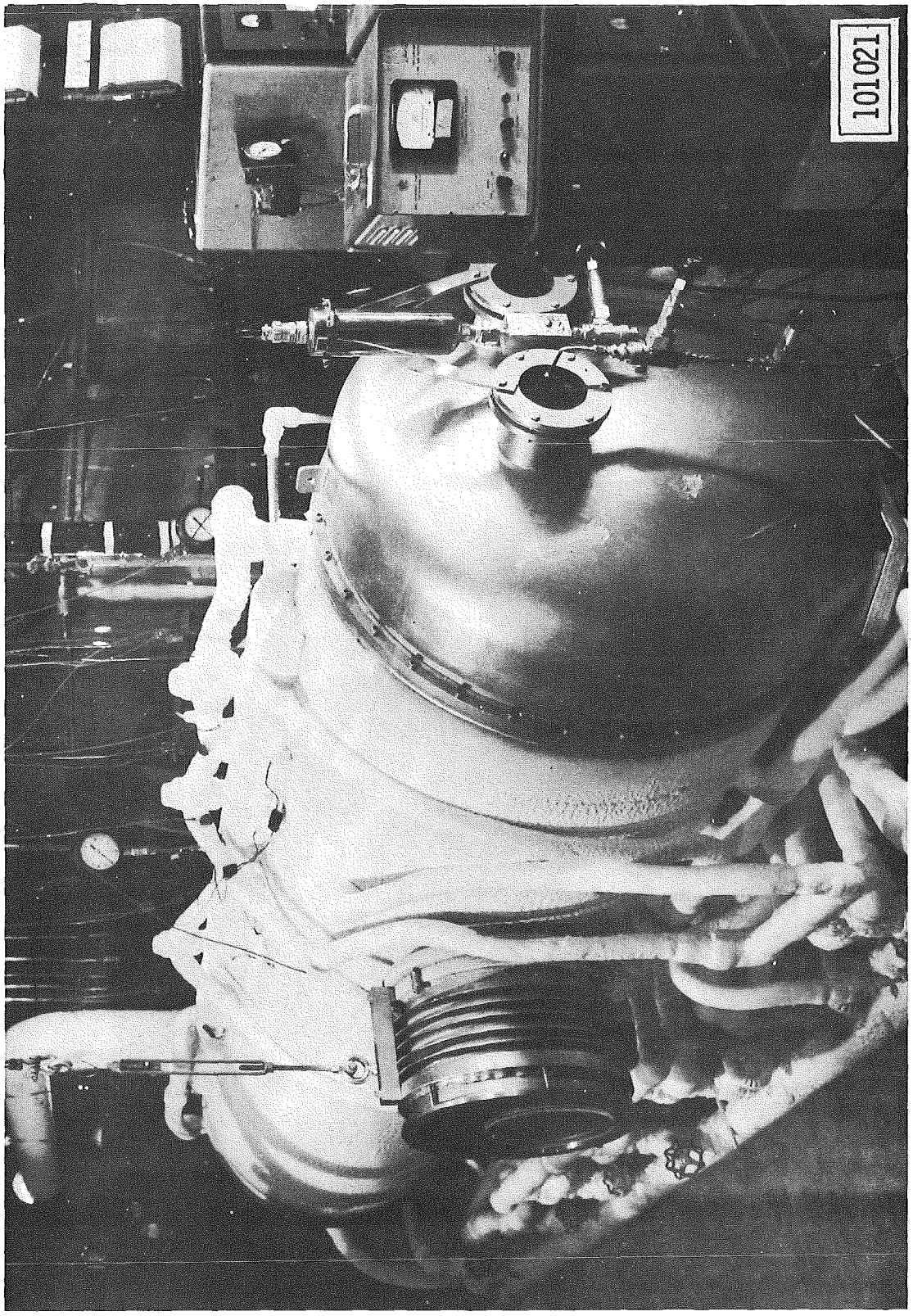

a. Cold Wall Vacuum Chamber

Fig. 2 Test Chamber Installation

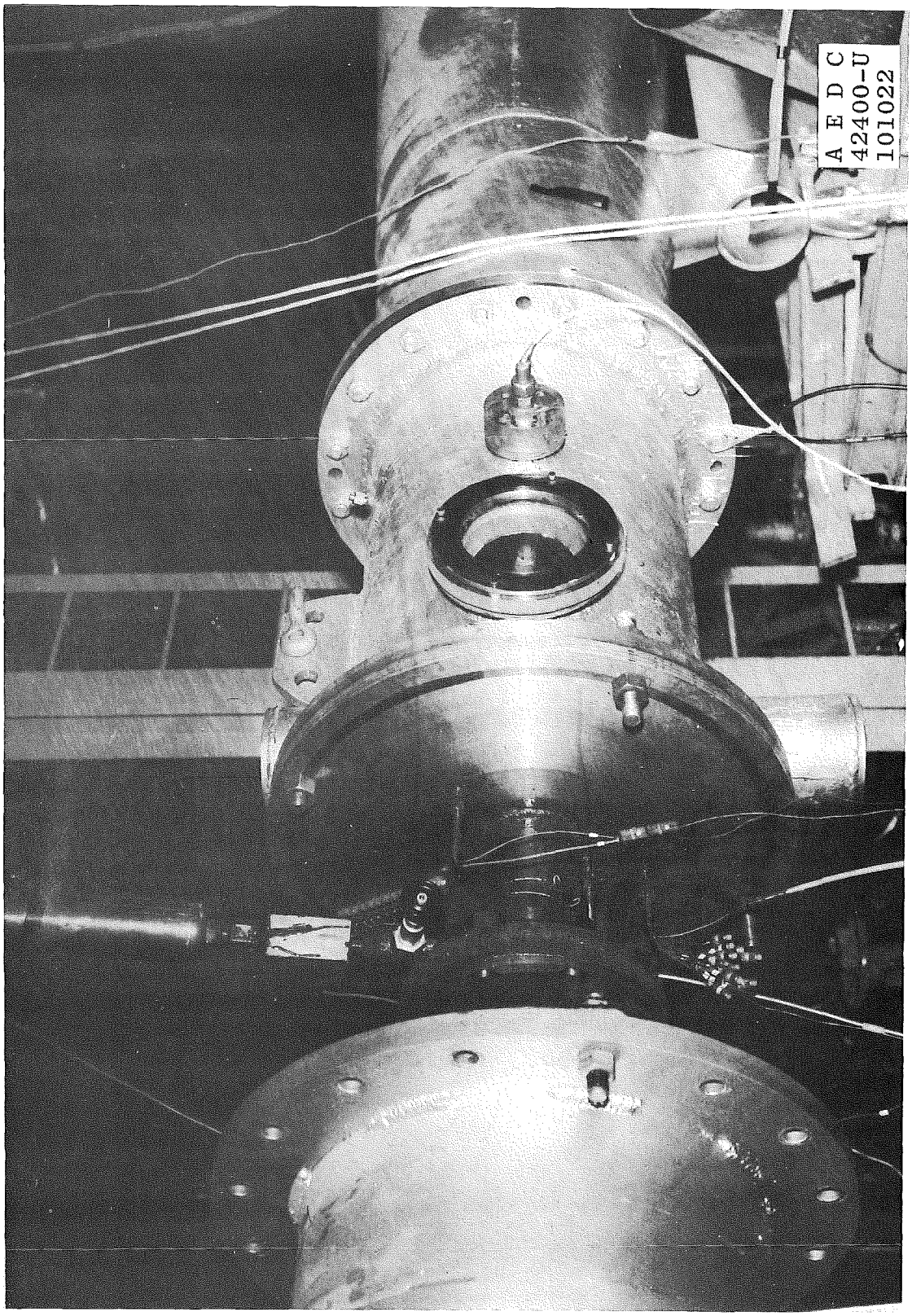

b. 18-in. Test Cell
Fig. 2 Concluded

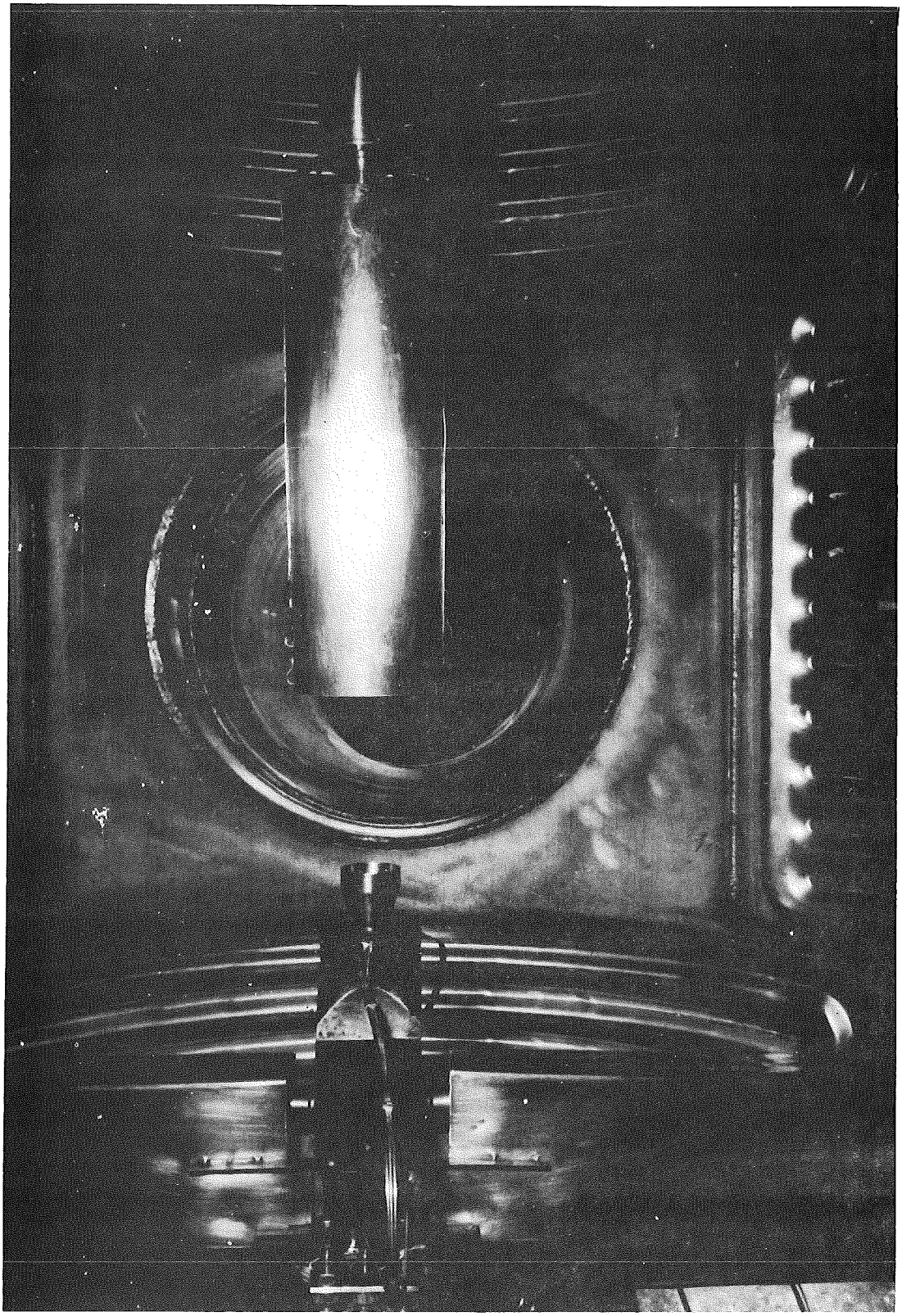

a. Cold Wall Vacuum Chamber

Fig. 3 Model Installation in the Test Chamber

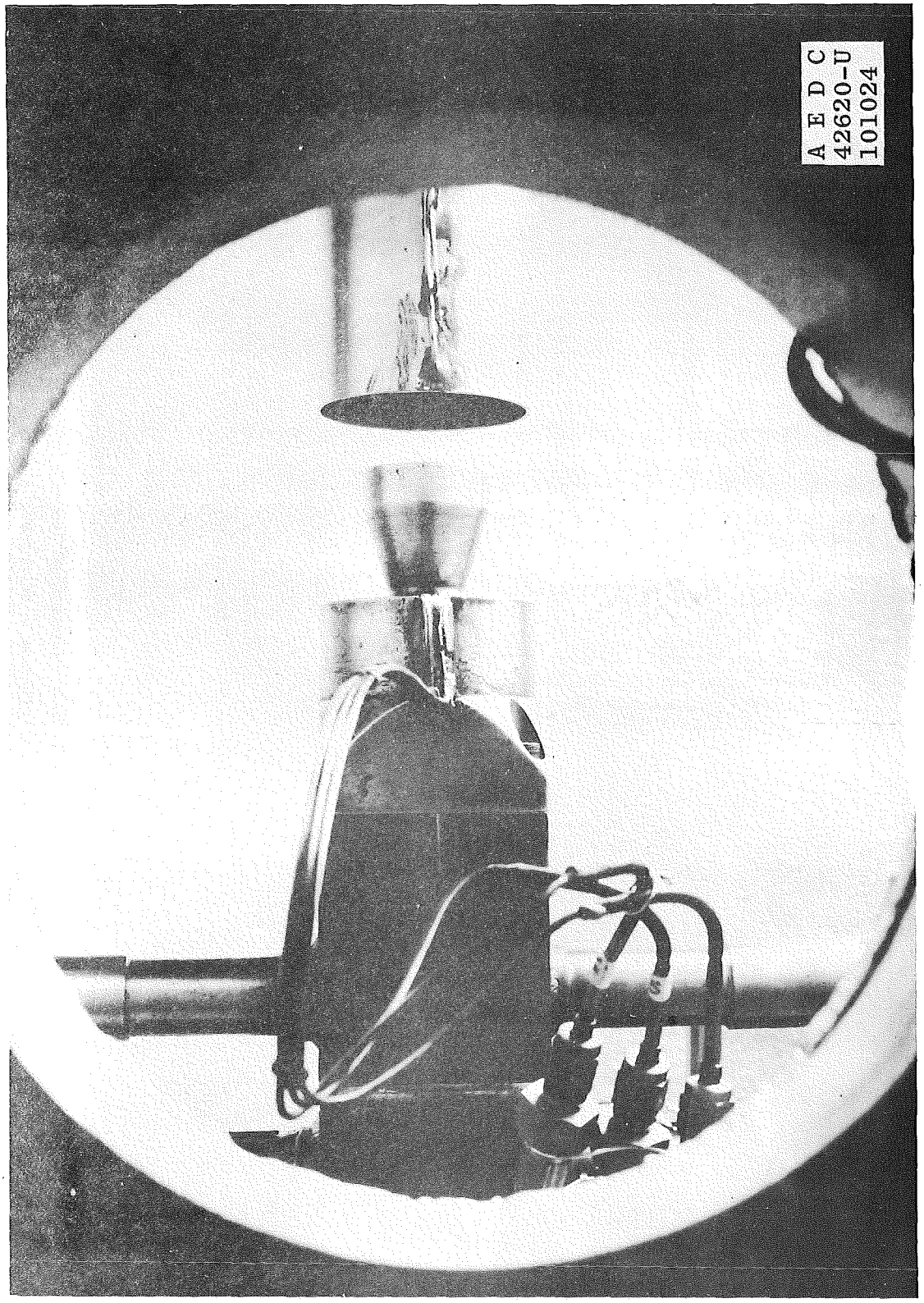

b. 18-in. Test Cell
Fig. 3 Concluded

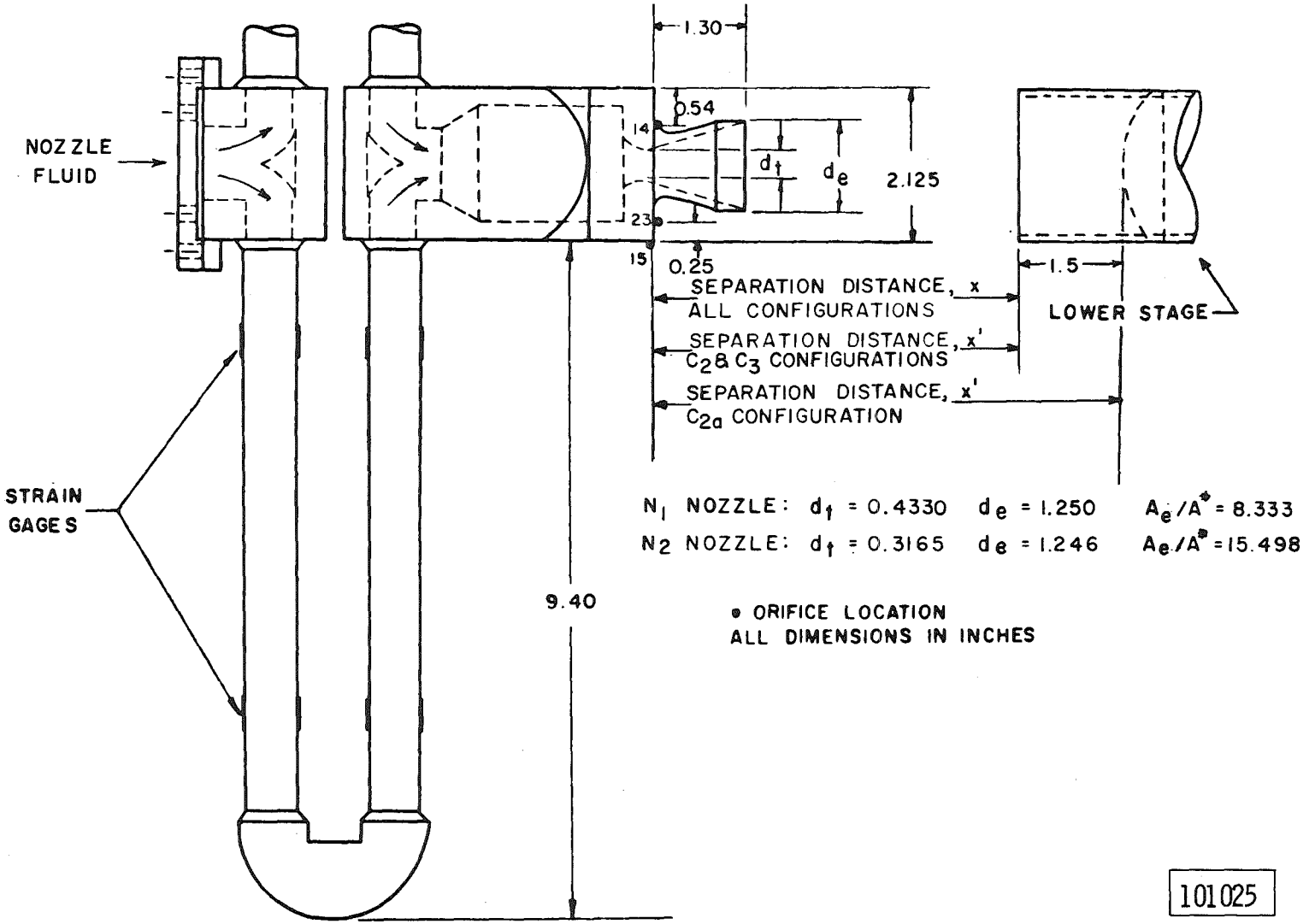

Fig. 4 Upper Stage Model Configurations

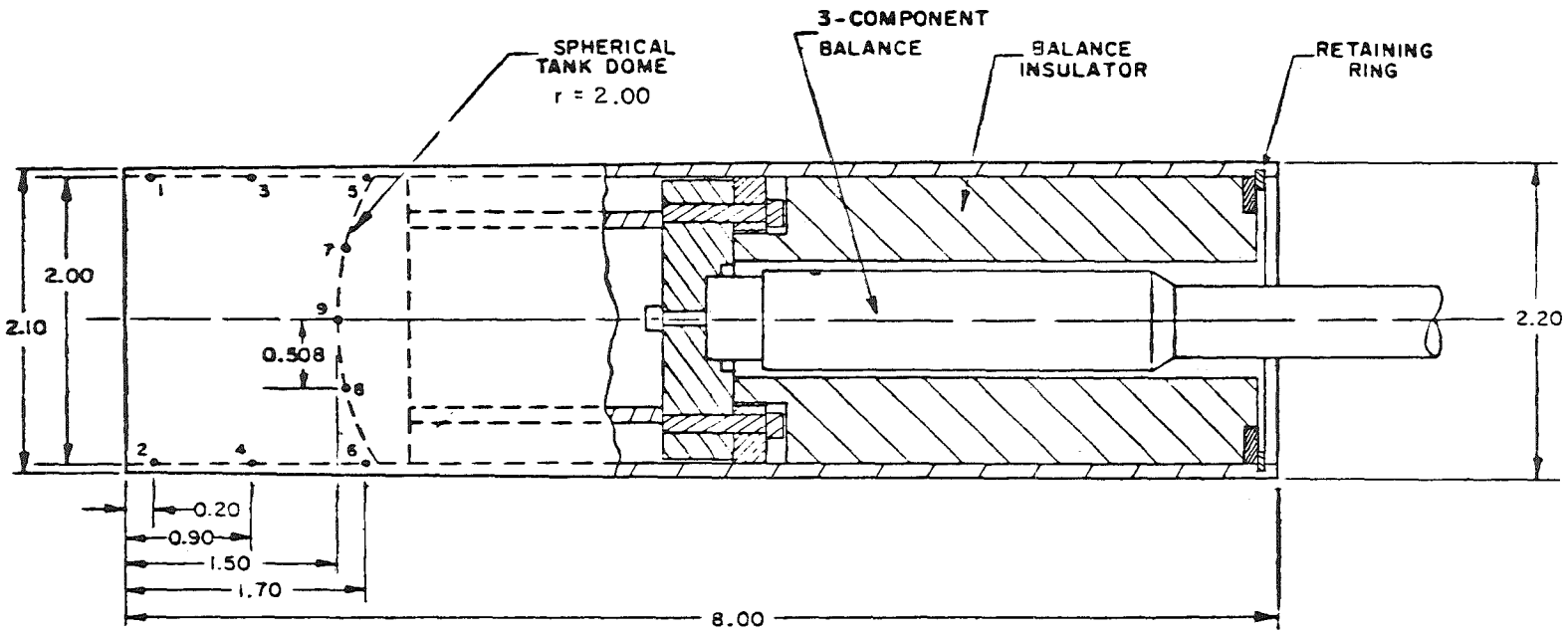

● ORIFICE LOCATION
ALL DIMENSIONS IN INCHES

101026

a. C_2 Configuration

Fig. 5 Lower Stage Model Configurations

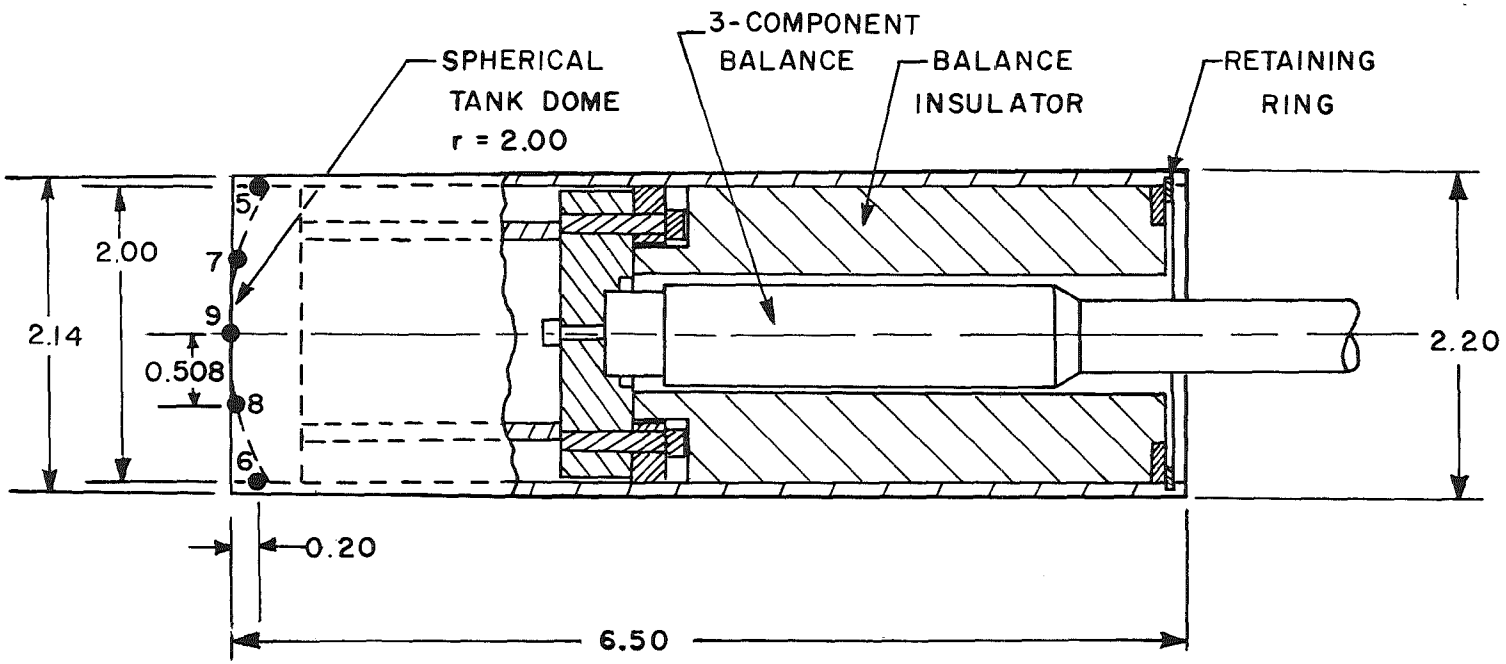

● ORIFICE LOCATION
ALL DIMENSIONS IN INCHES

101027

b. C_{2a} Configuration
Fig. 5 Continued

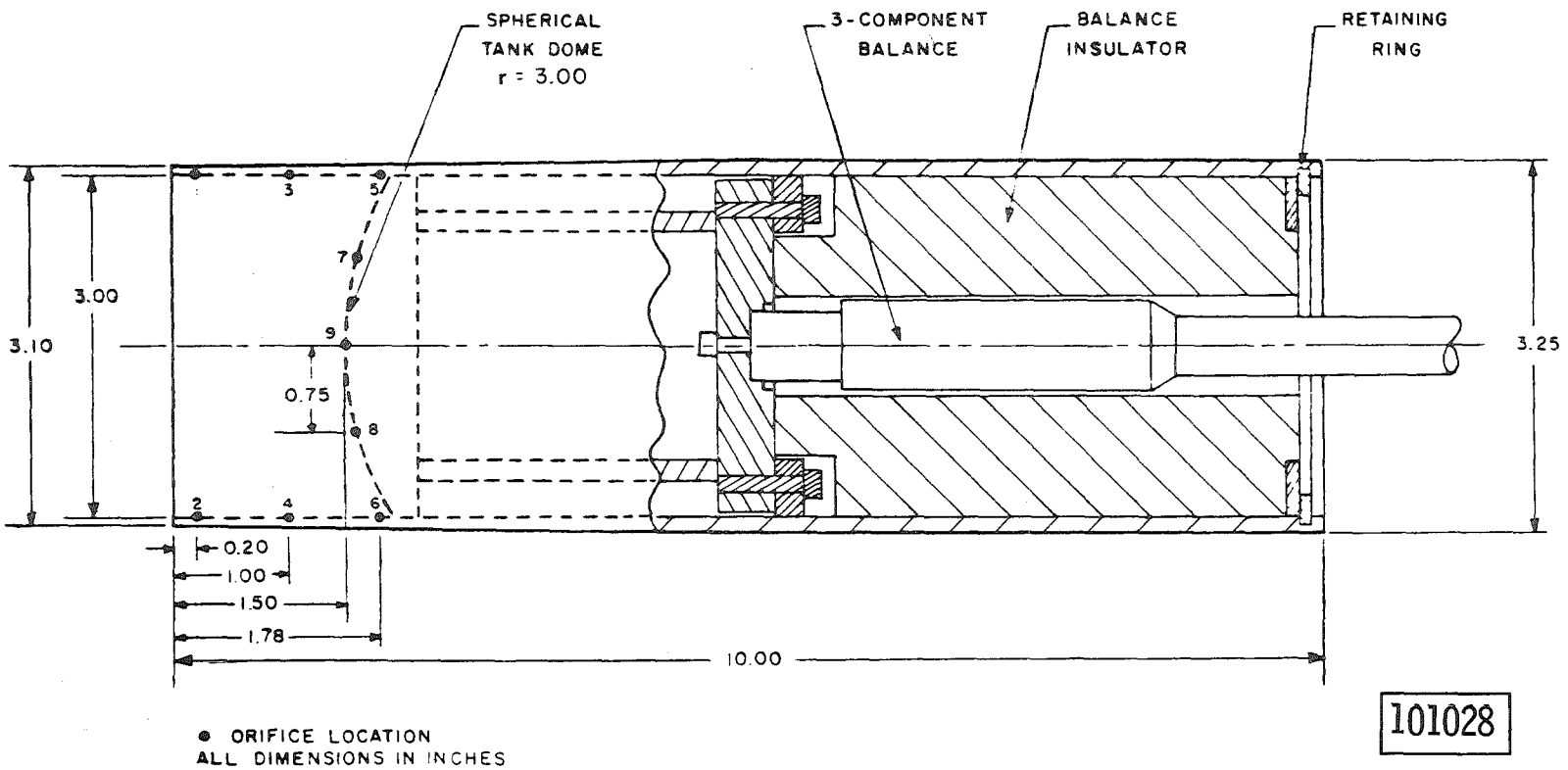

c. C_3 Configuration

Fig. 5 Concluded

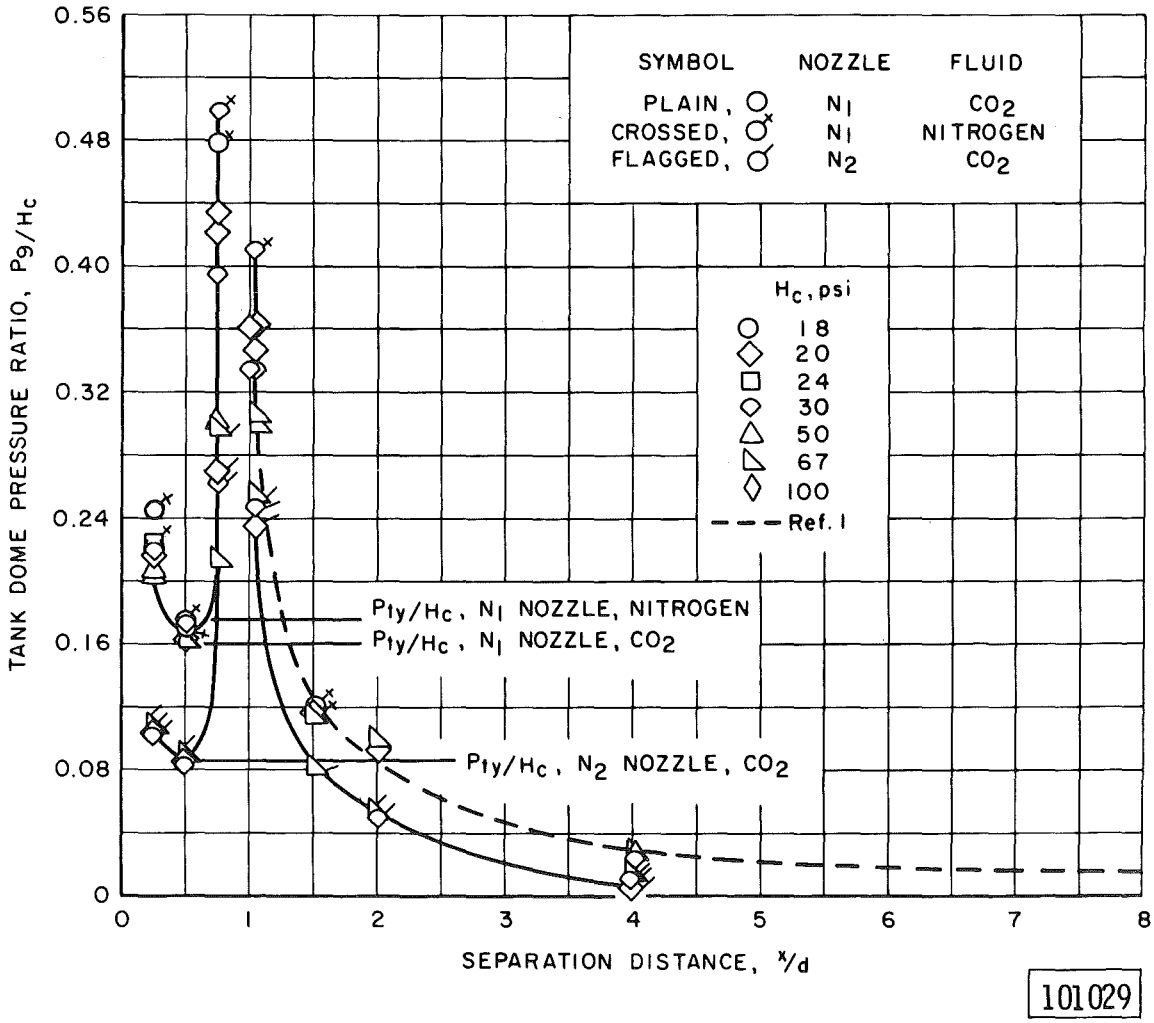

a. C_2 Configuration

Fig. 6 The Effect of Separation Distance and Upper Stage Configuration on Tank Dome Pressure Ratio

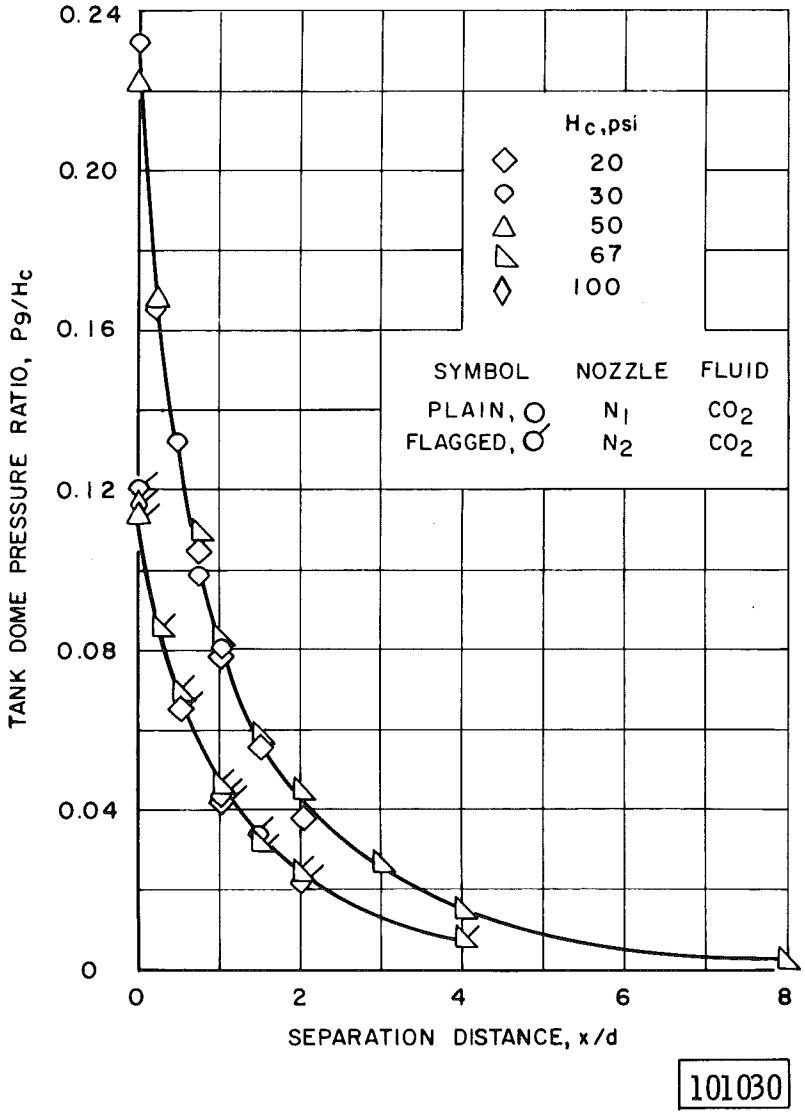

b. C_{2a} Configuration

Fig. 6 Continued

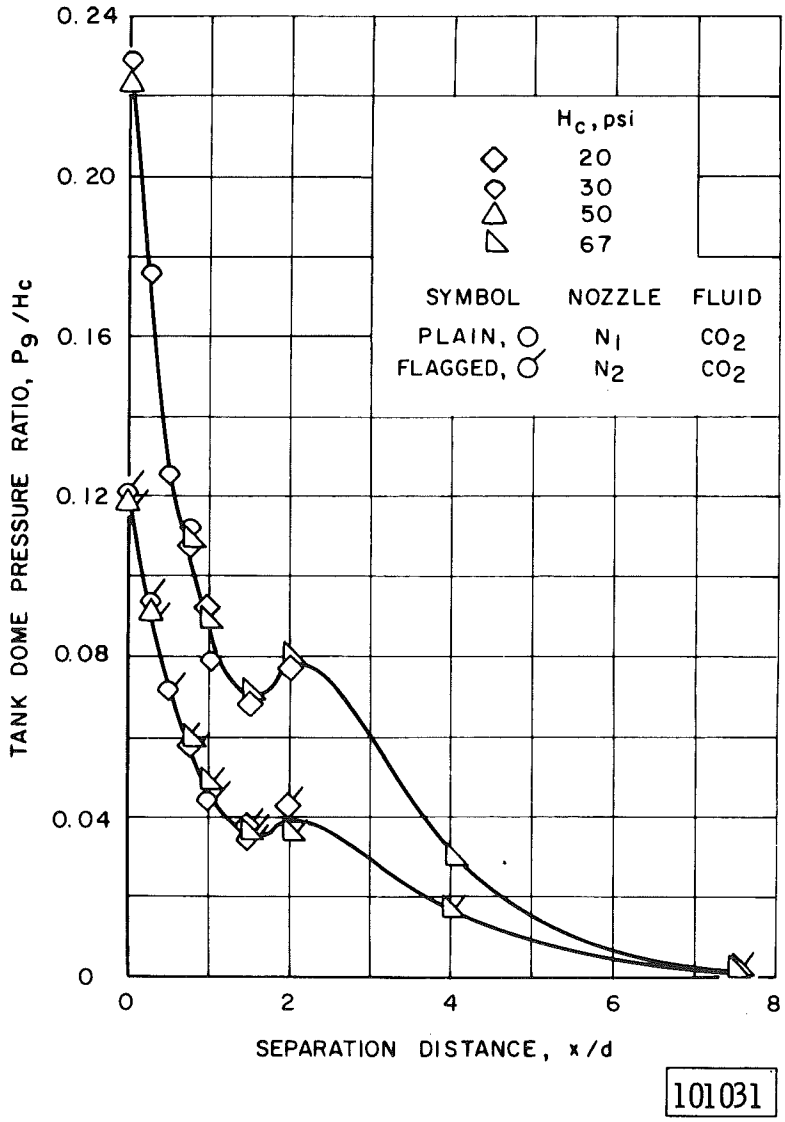

c. C_3 Configuration
Fig. 6 Concluded

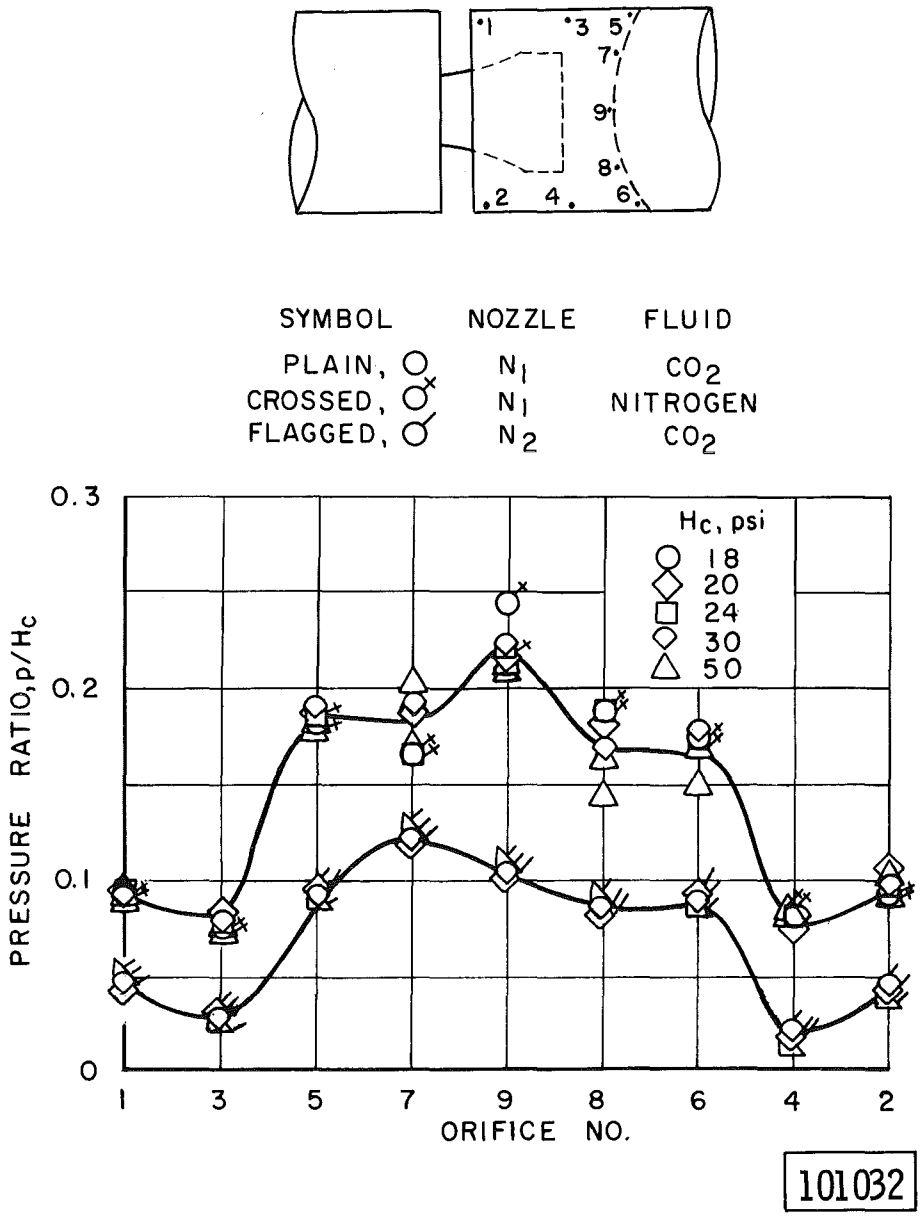

a. x/d = 0.25

Fig. 7 Lower Stage Static Pressure Distribution, C_2 Configuration

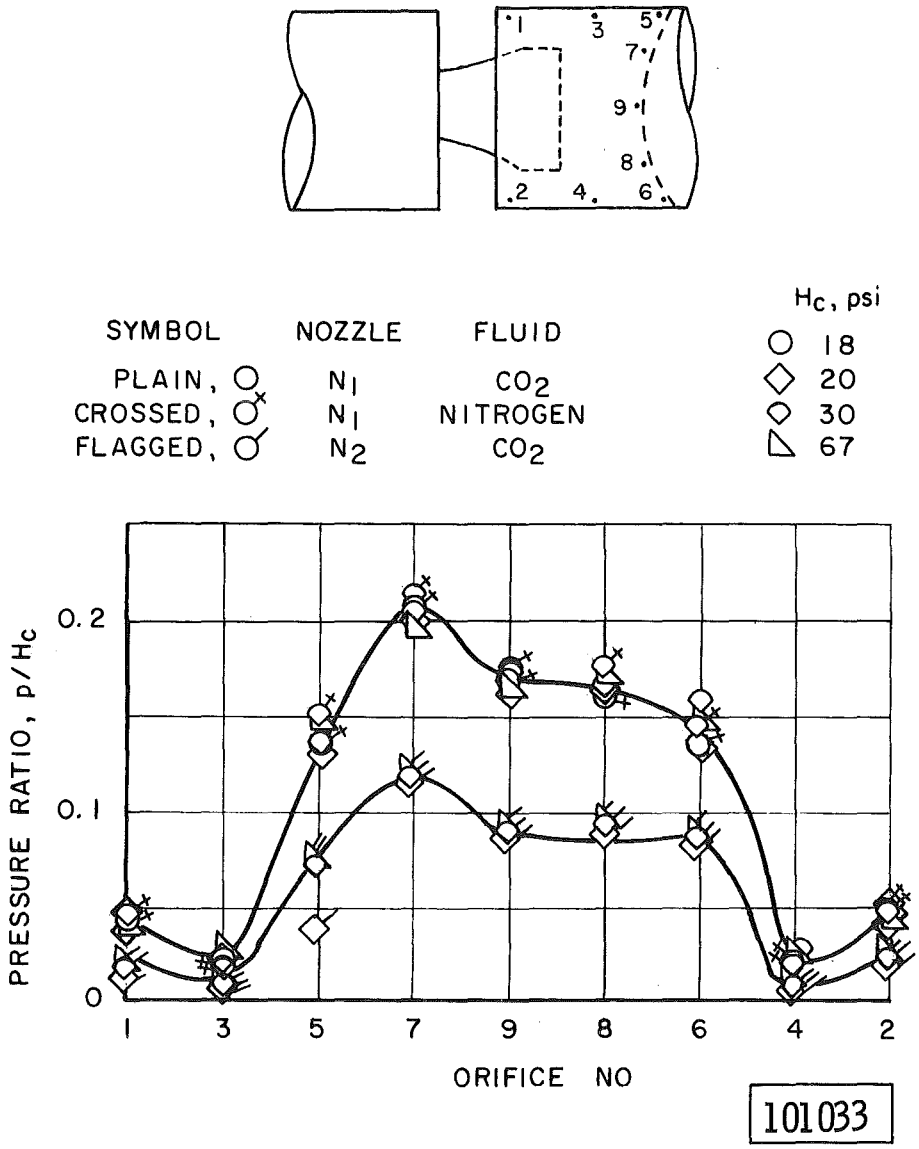

b. x/d = 0.50

Fig. 7 Continued

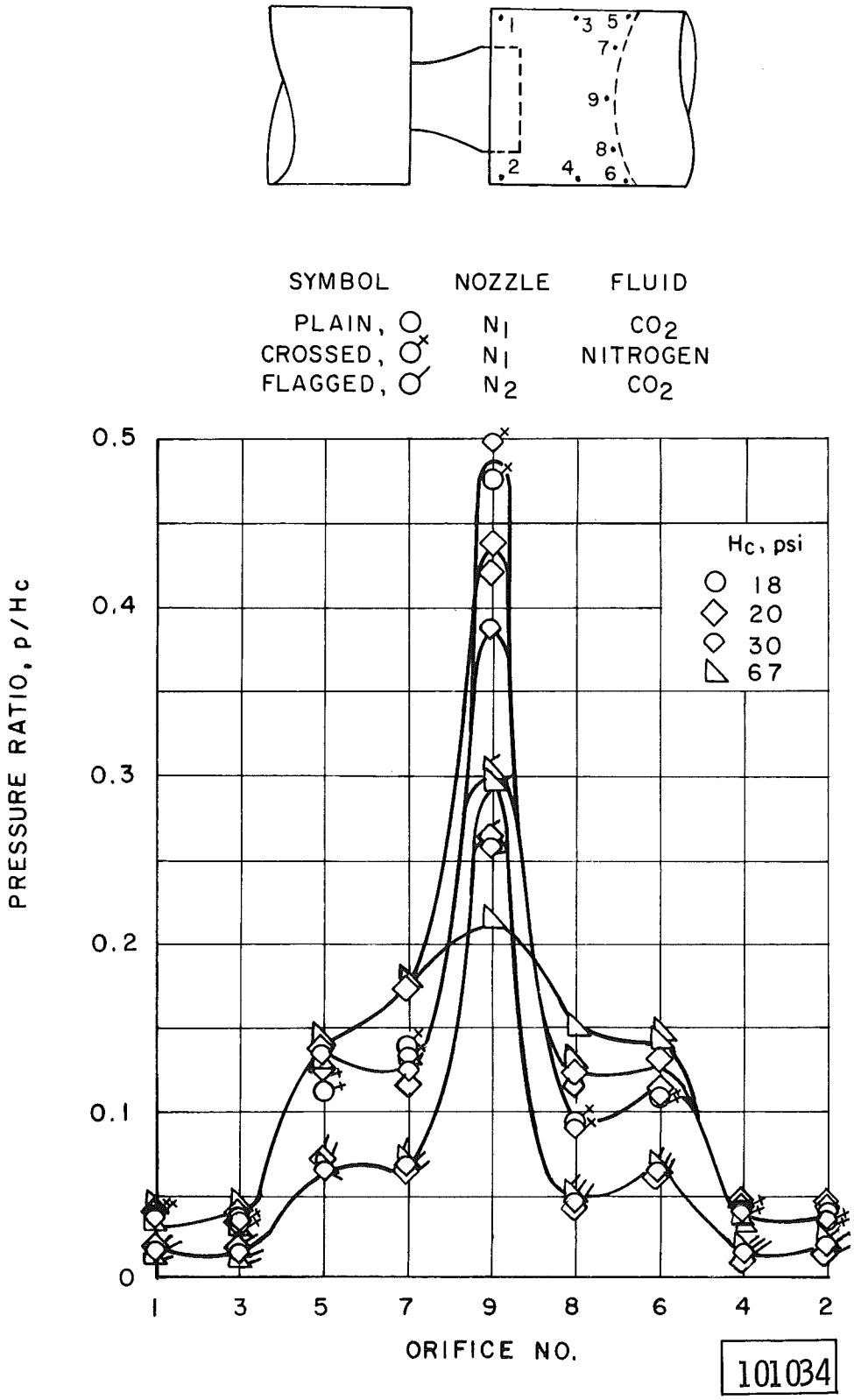

c. x/d = 0.75

Fig. 7 Continued

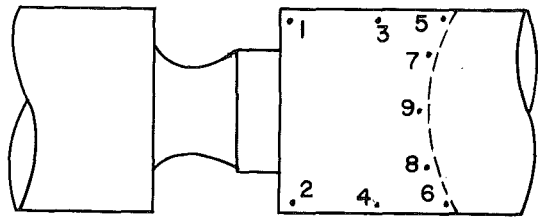

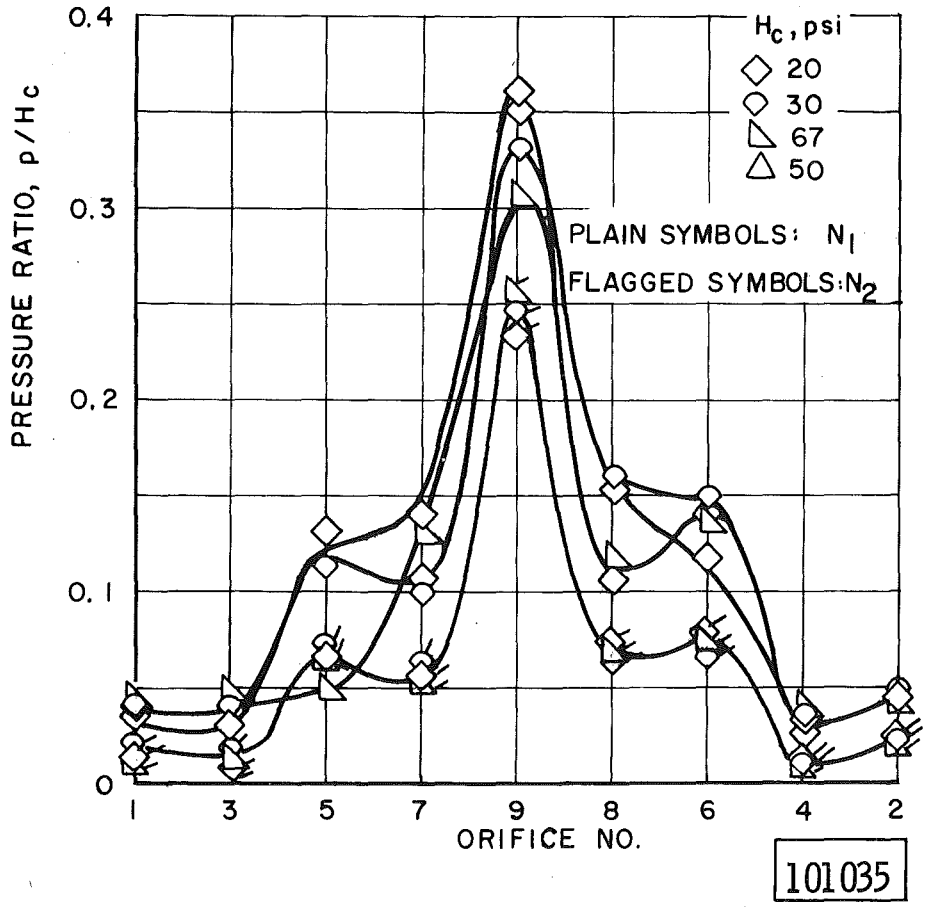

d. x/d = 1.04

Fig. 7 Continued

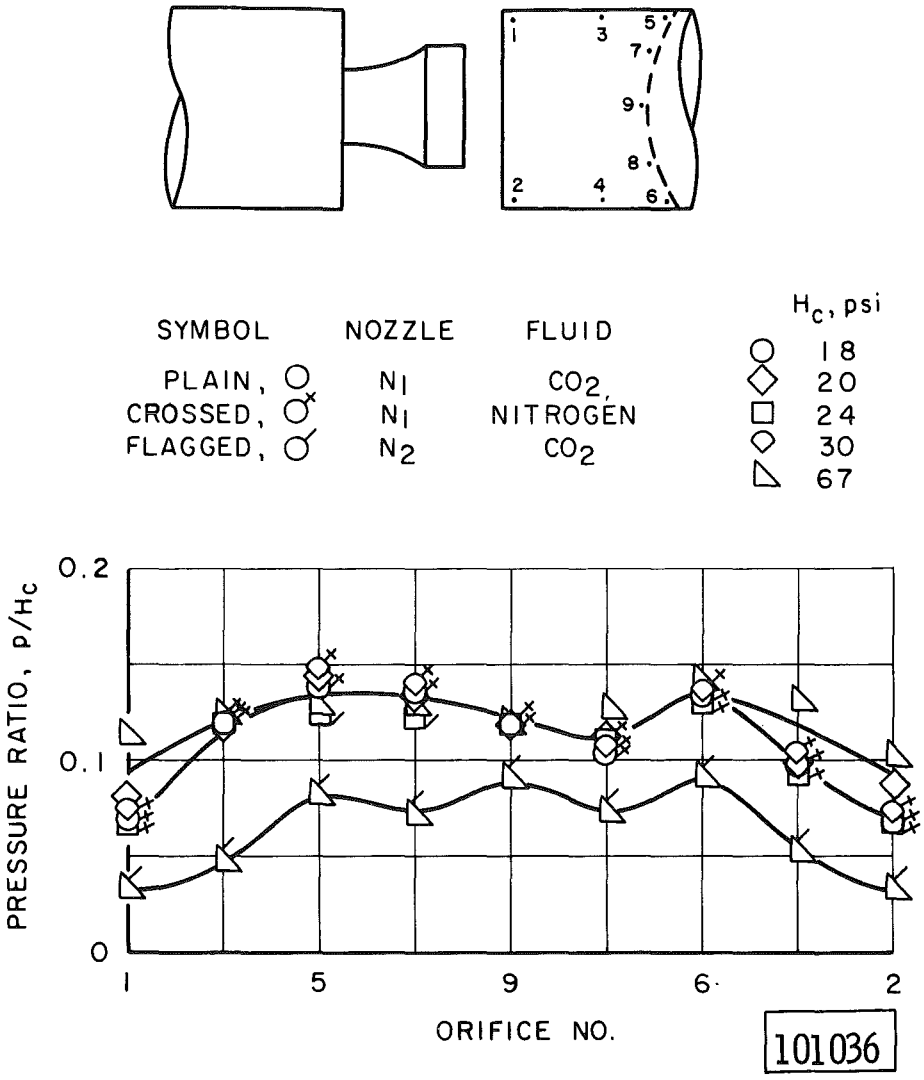

e. x/d = 1.50

Fig. 7 Continued

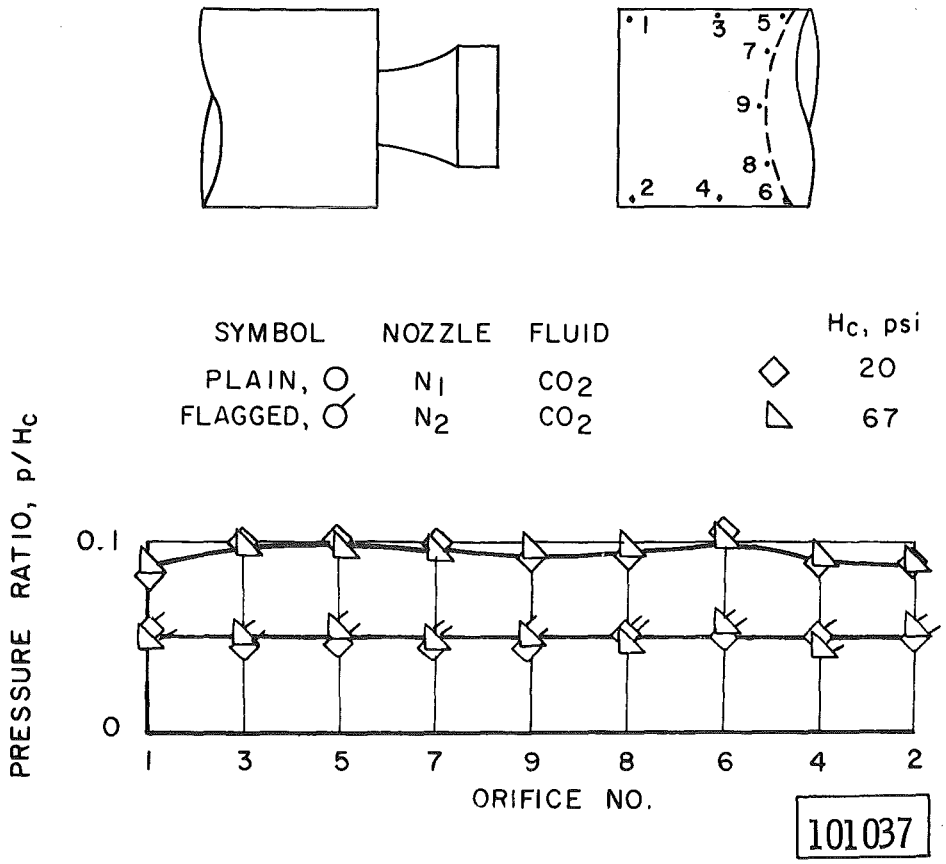

f. x/d = 2.00

Fig. 7 Concluded

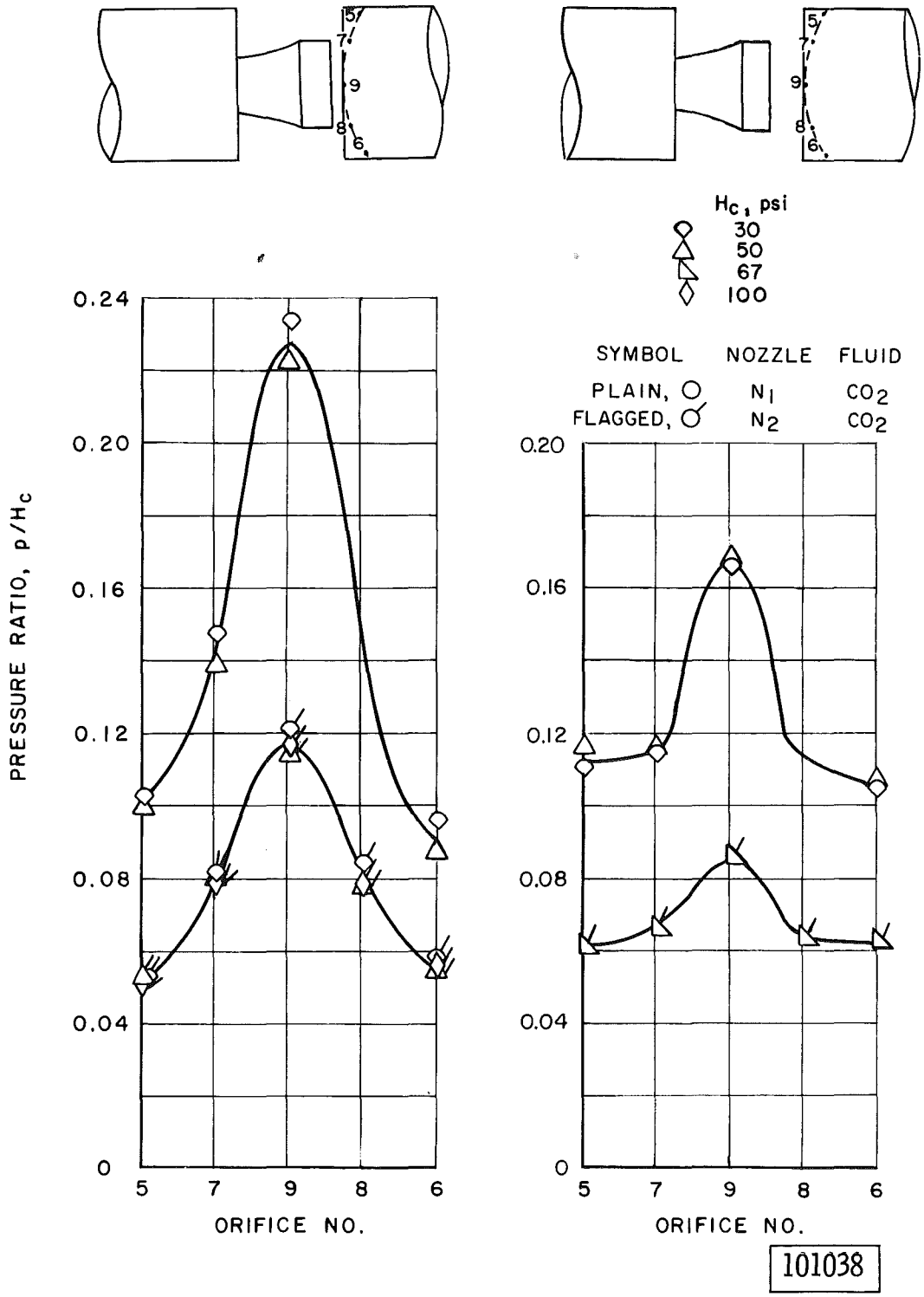

a. x/d = 0

b. x/d = 0.25

Fig. 8 Lower Stage Static Pressure Distribution, C_{2a} Configuration

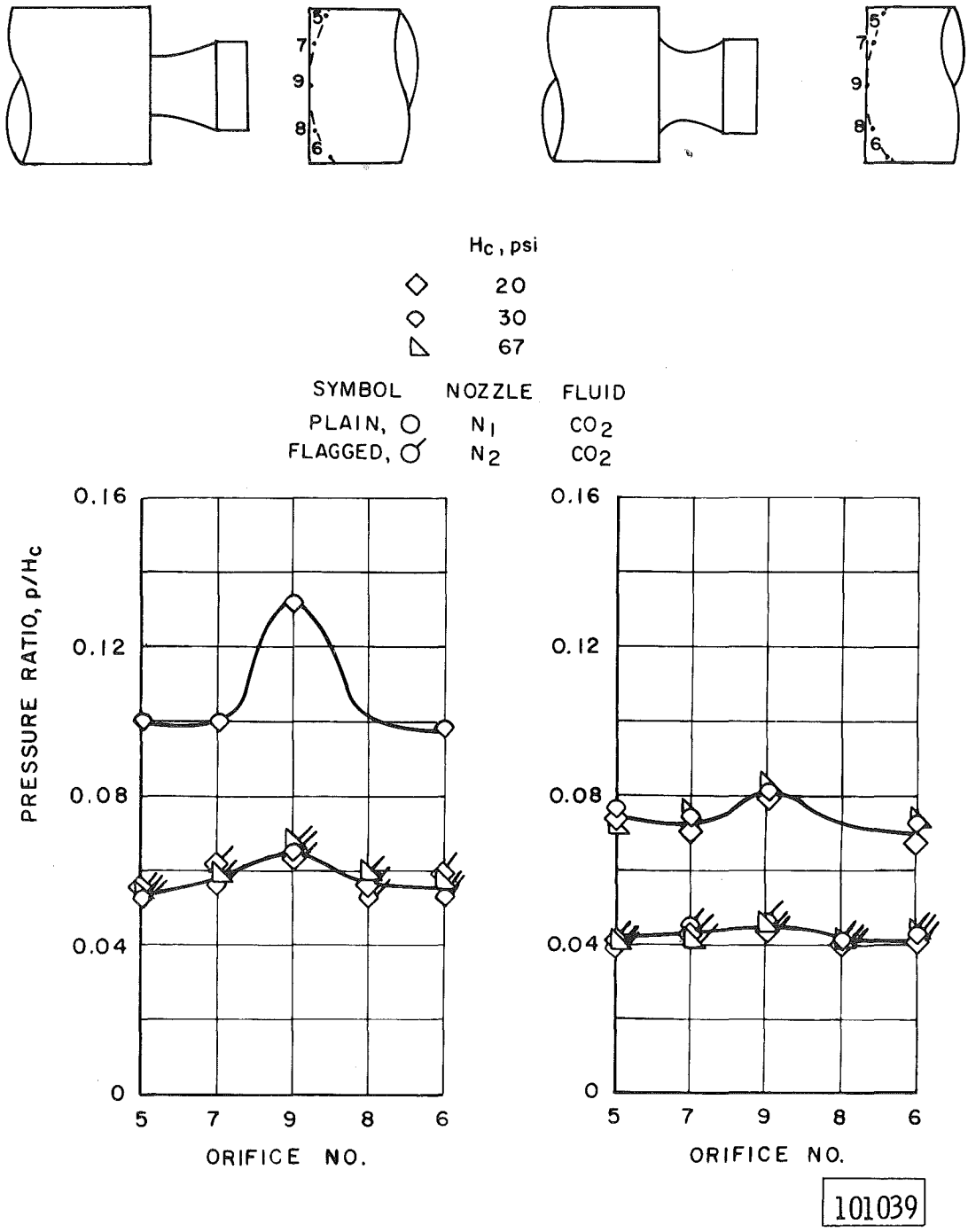

c. x/d = 0.50

d. x/d = 1.04

Fig. 8 Concluded

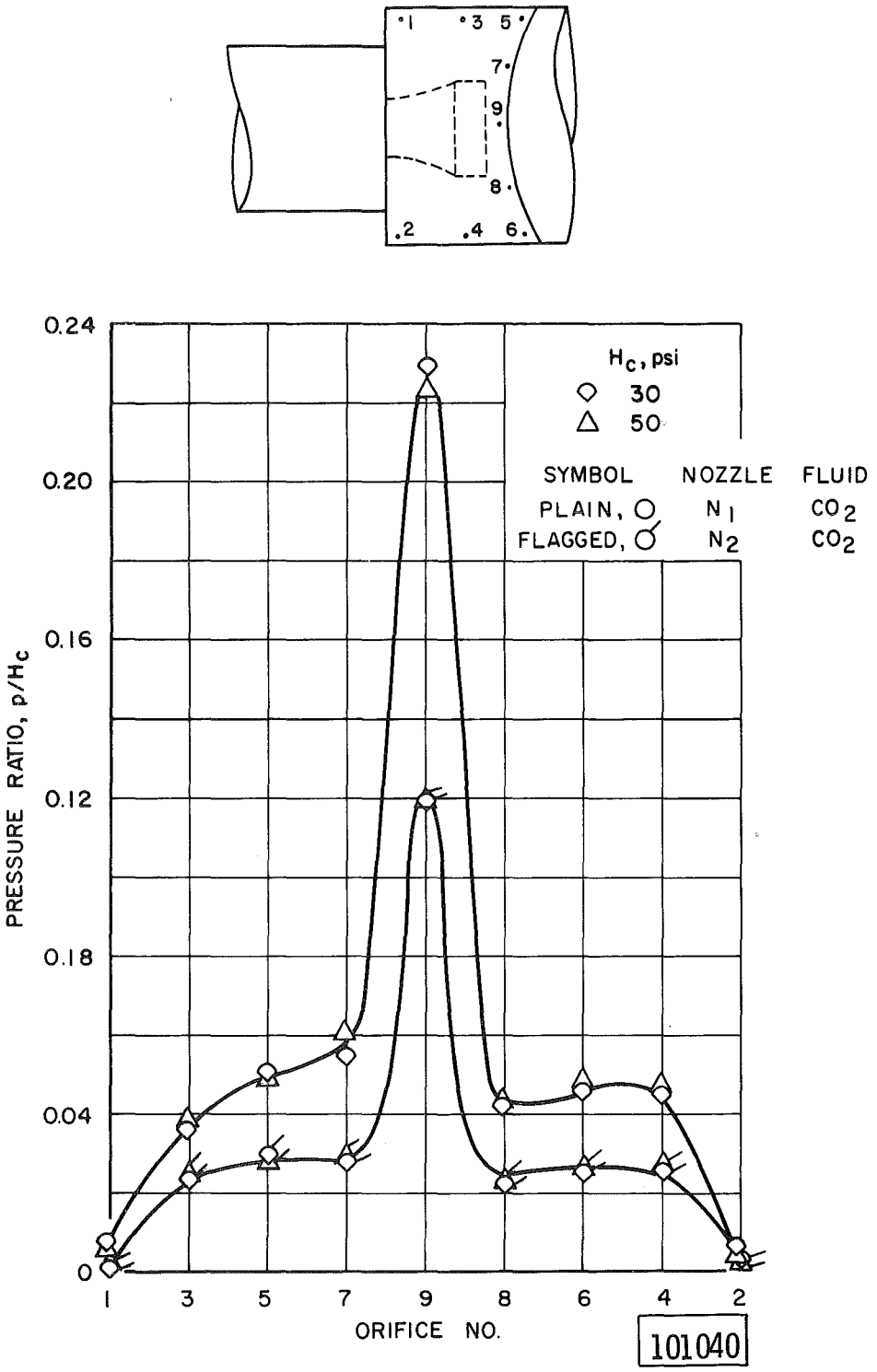

a. x/d = 0

Fig. 9 Lower Stage Static Pressure Distribution, C_3 Configuration

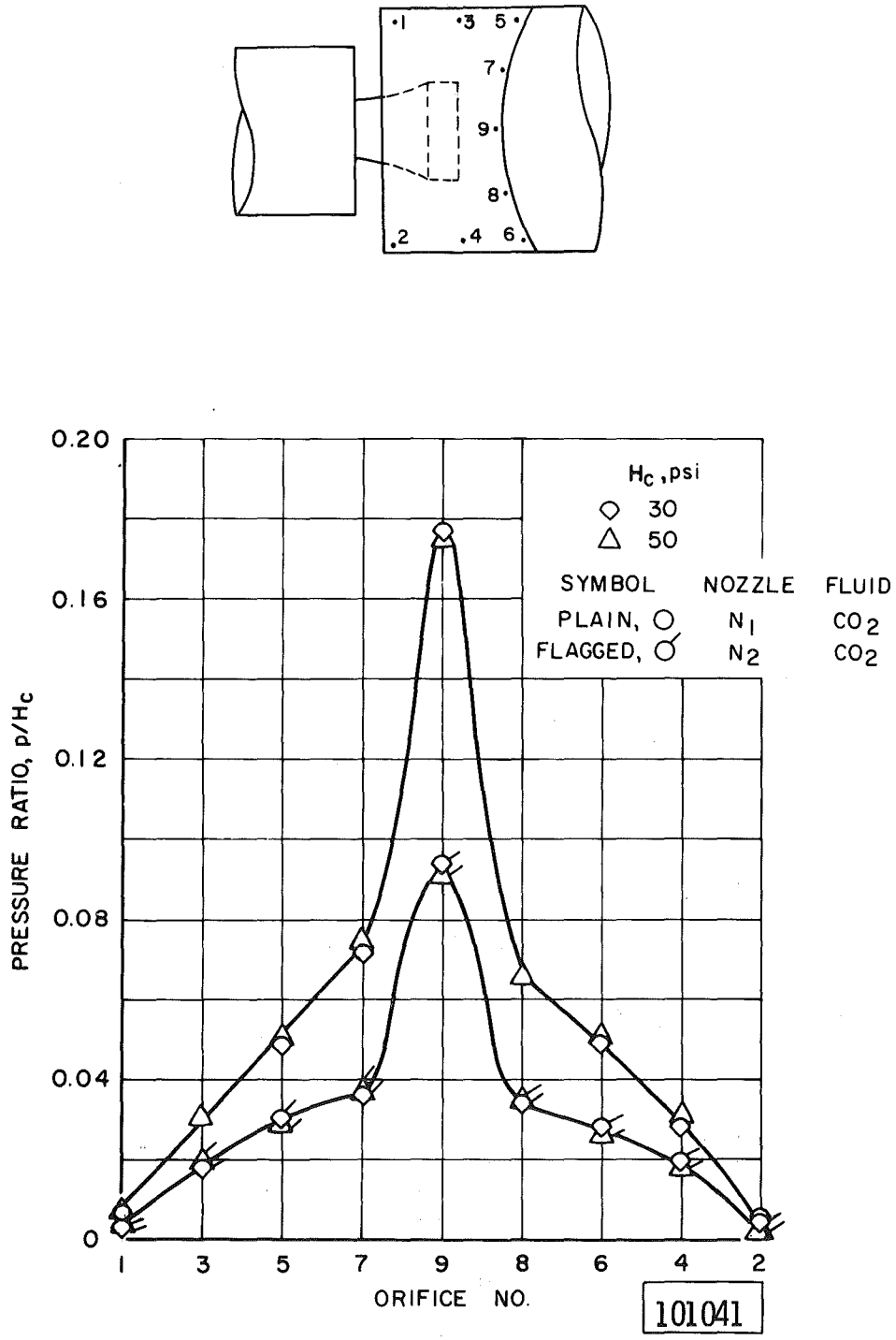

b. x/d = 0.25

Fig. 9 Continued

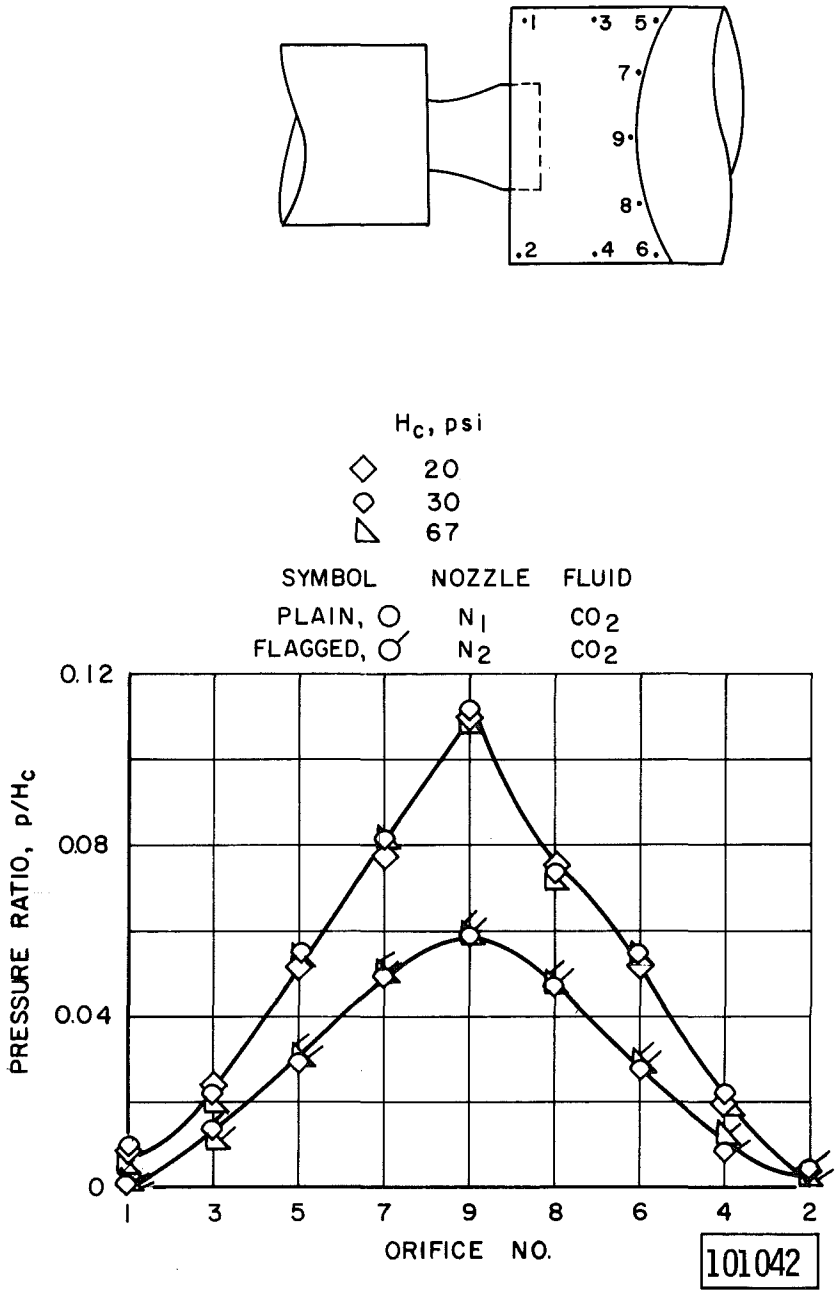

c. x/d = 0.75

Fig. 9 Continued

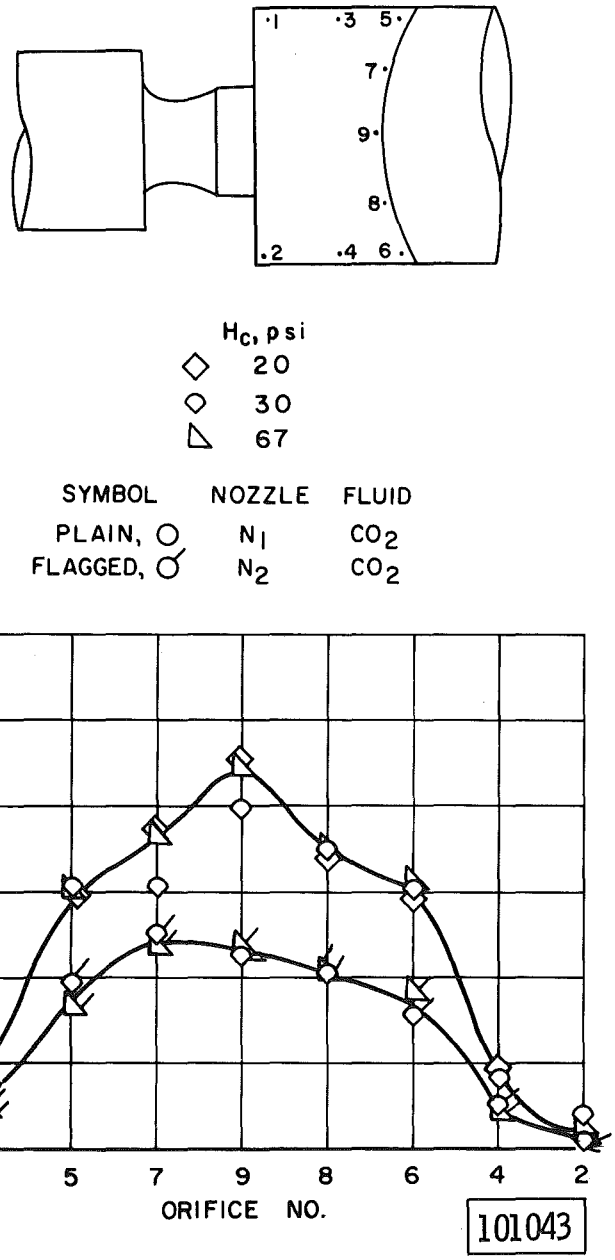

d. x/d = 1.04

Fig. 9 Continued

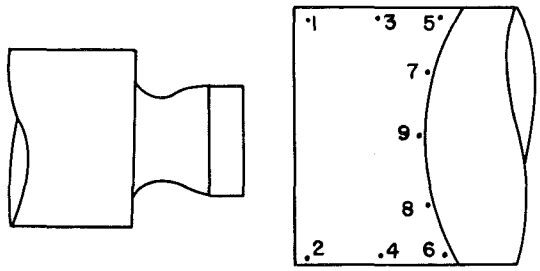

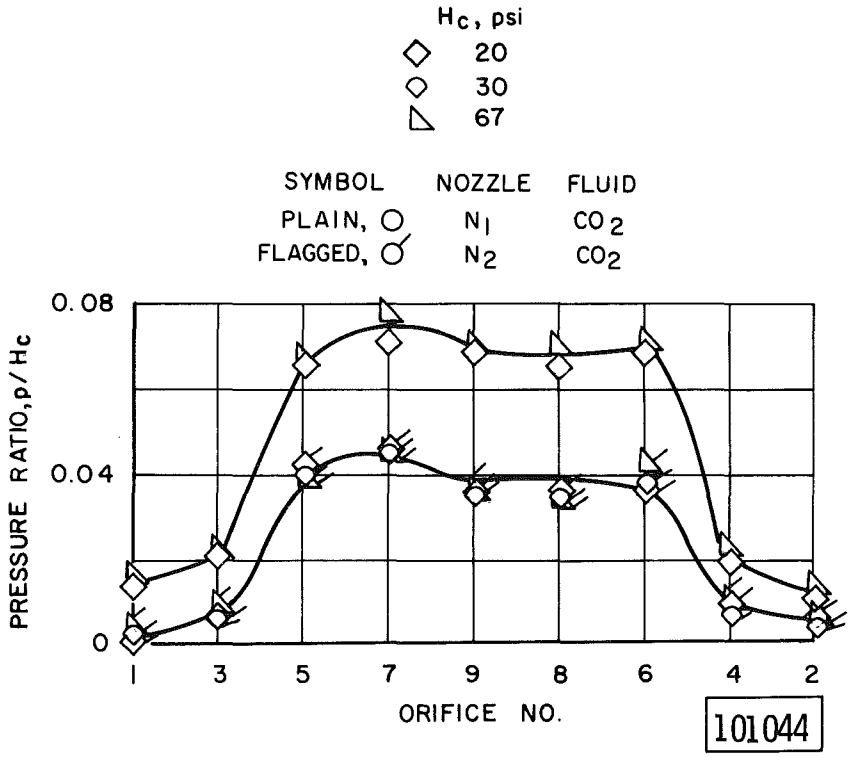

e. x/d = 1.50

Fig. 9 Continued

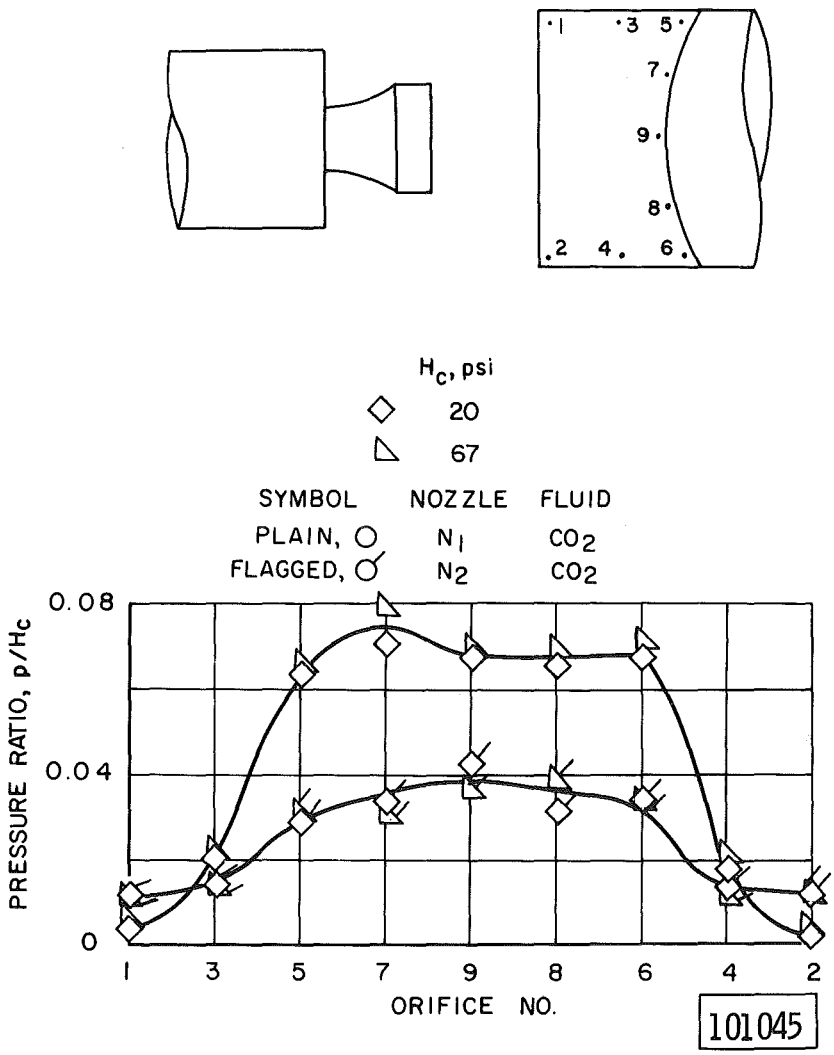

f. x/d = 2.00

Fig. 9 Continued

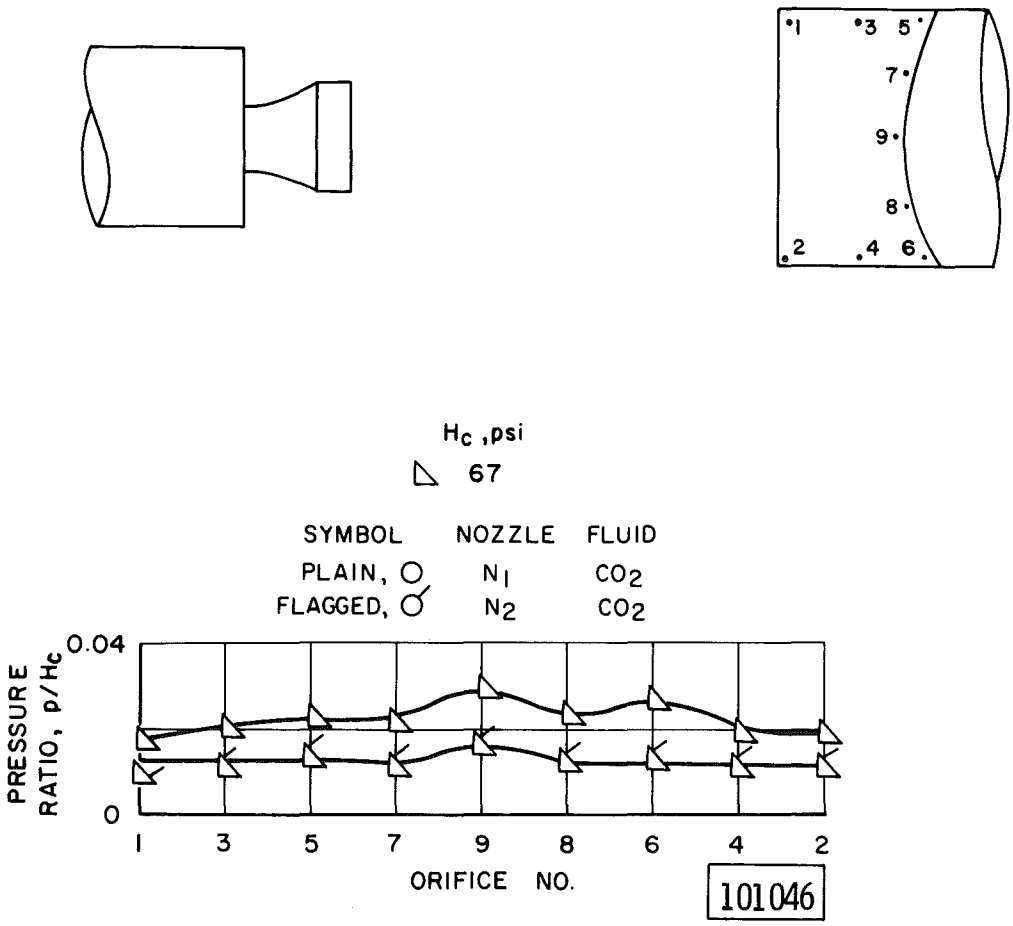

g. x/d = 4.00

Fig. 9 Concluded

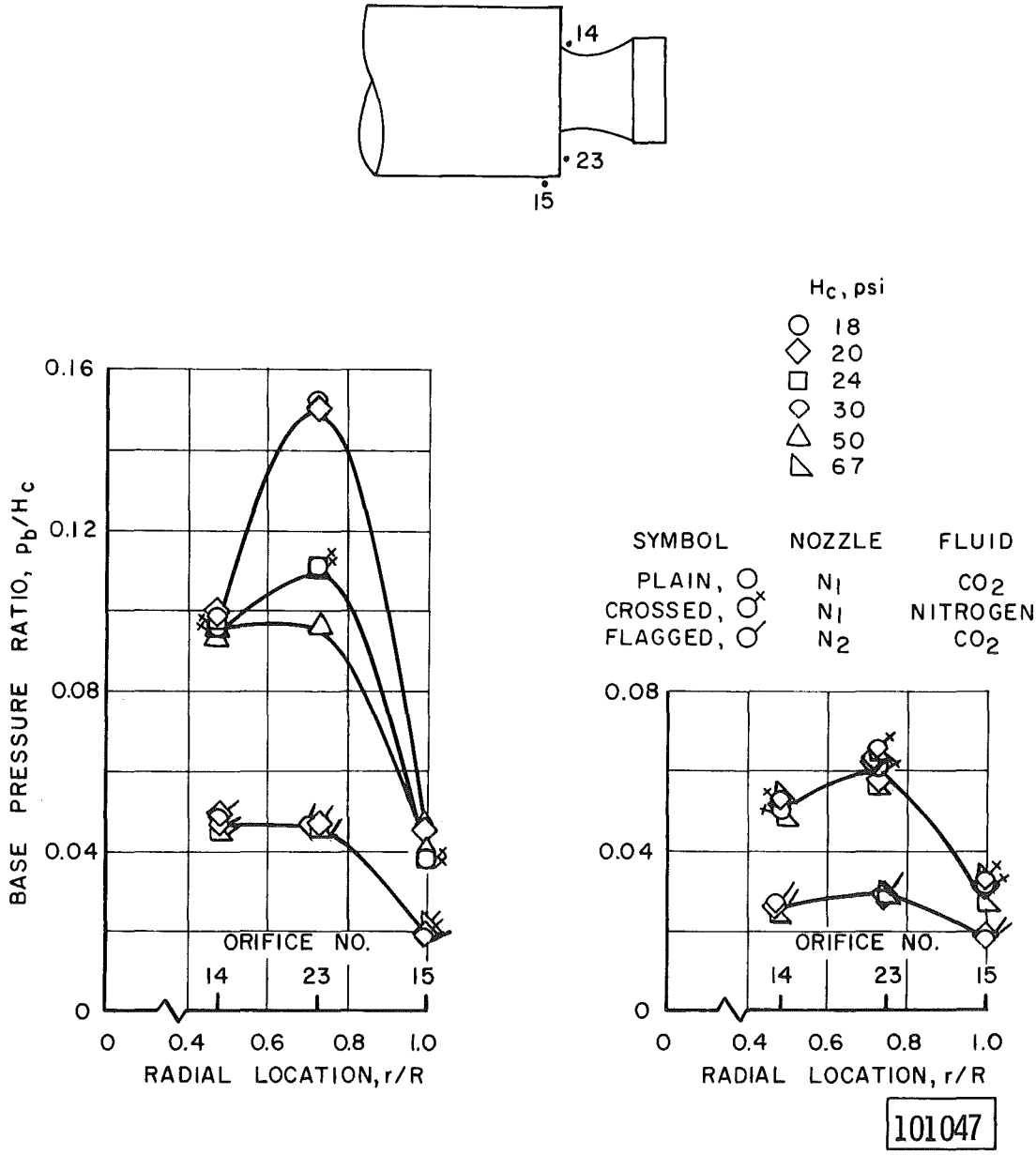

a. x/d = 0.25

b. x/d = 0.50

Fig. 10 Upper Stage Base Pressure Distribution with C_2 Configuration

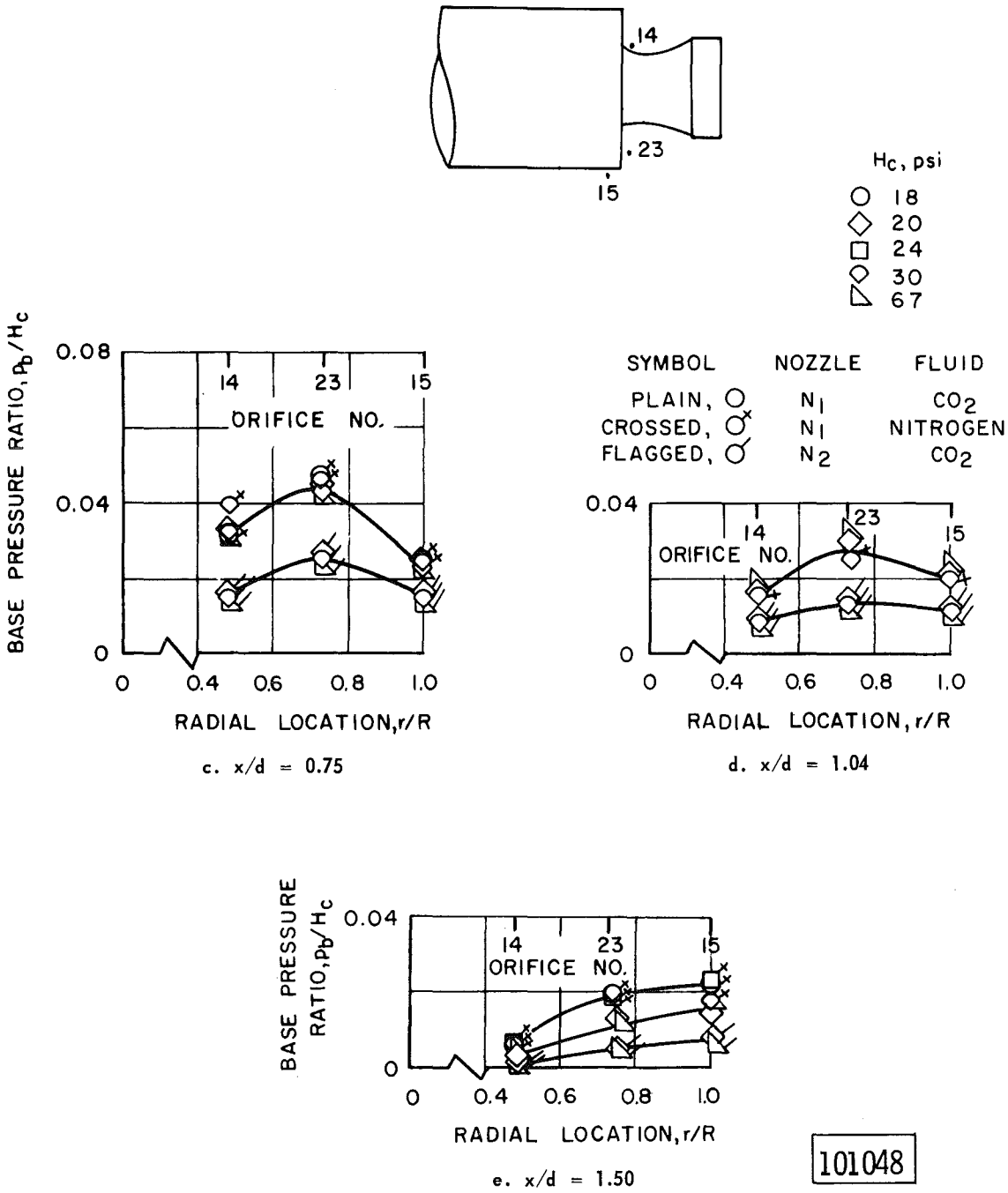

Fig. 10 Concluded

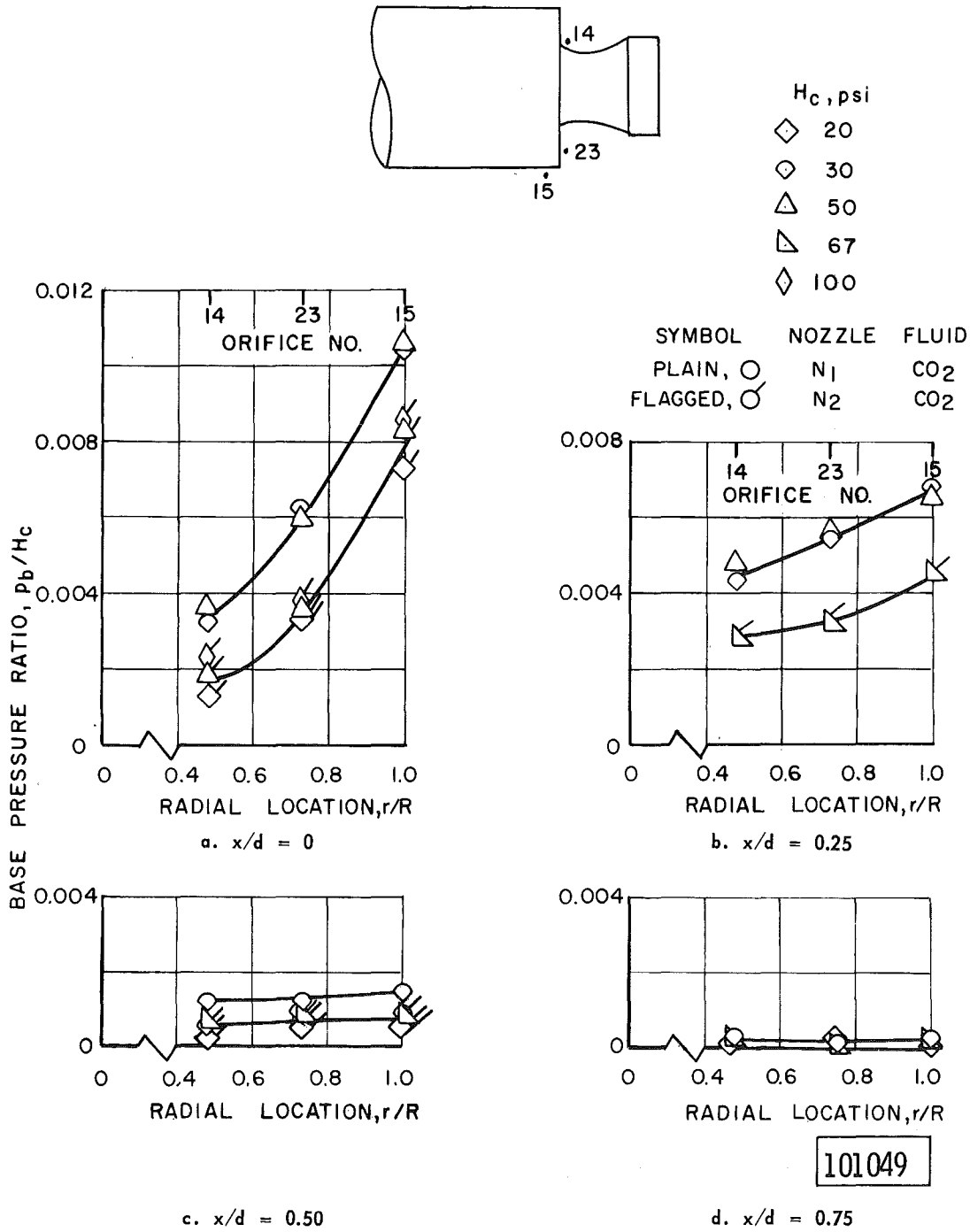

Fig. 11 Upper Stage Base Pressure Distribution with C_{2a} Configuration

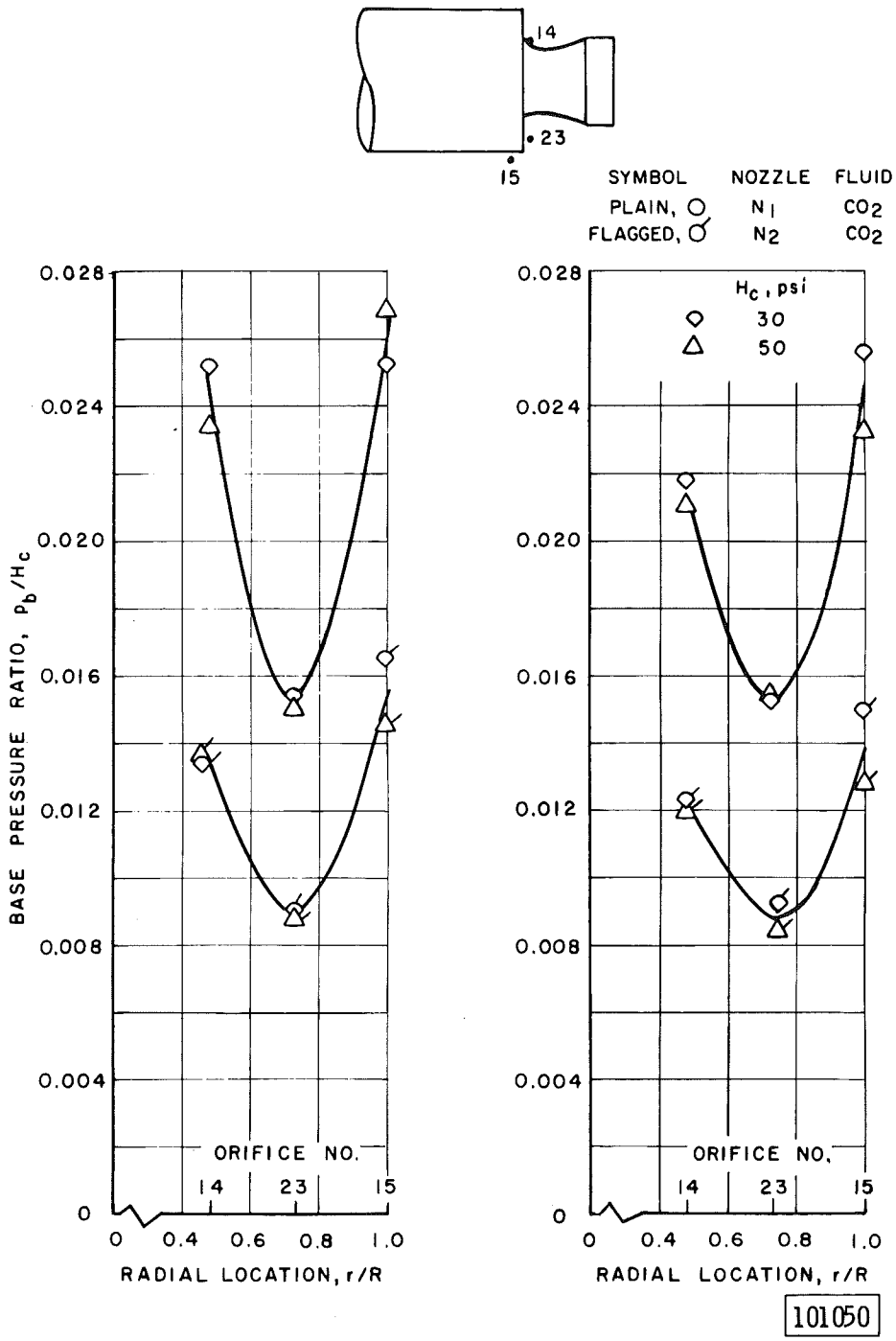

a. x/d = 0

b. x/d = 0.25

Fig. 12 Upper Stage Base Pressure Distribution with C_3 Configuration

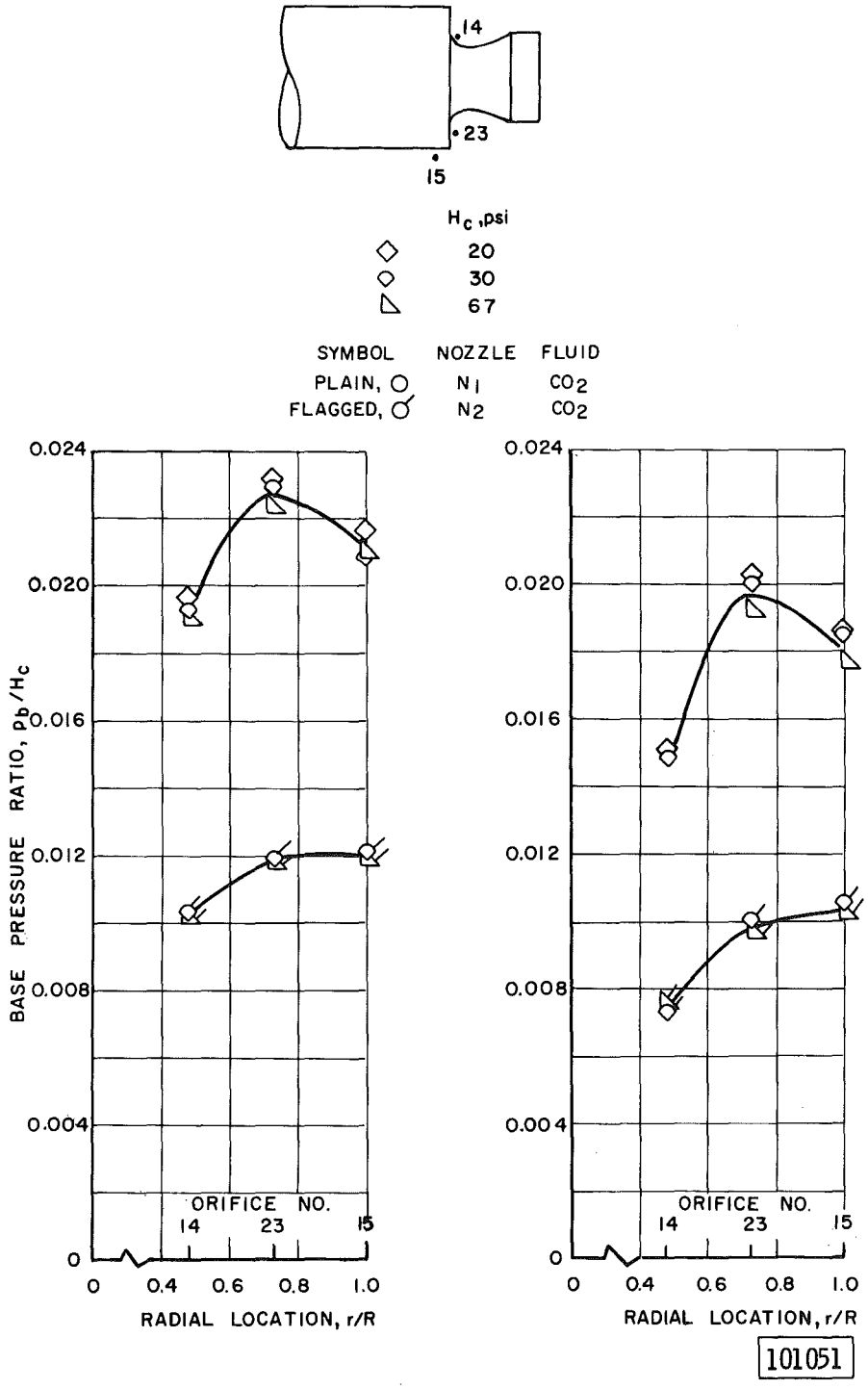

c. x/d = 0.75

d. x/d = 1.04

Fig. 12 Continued

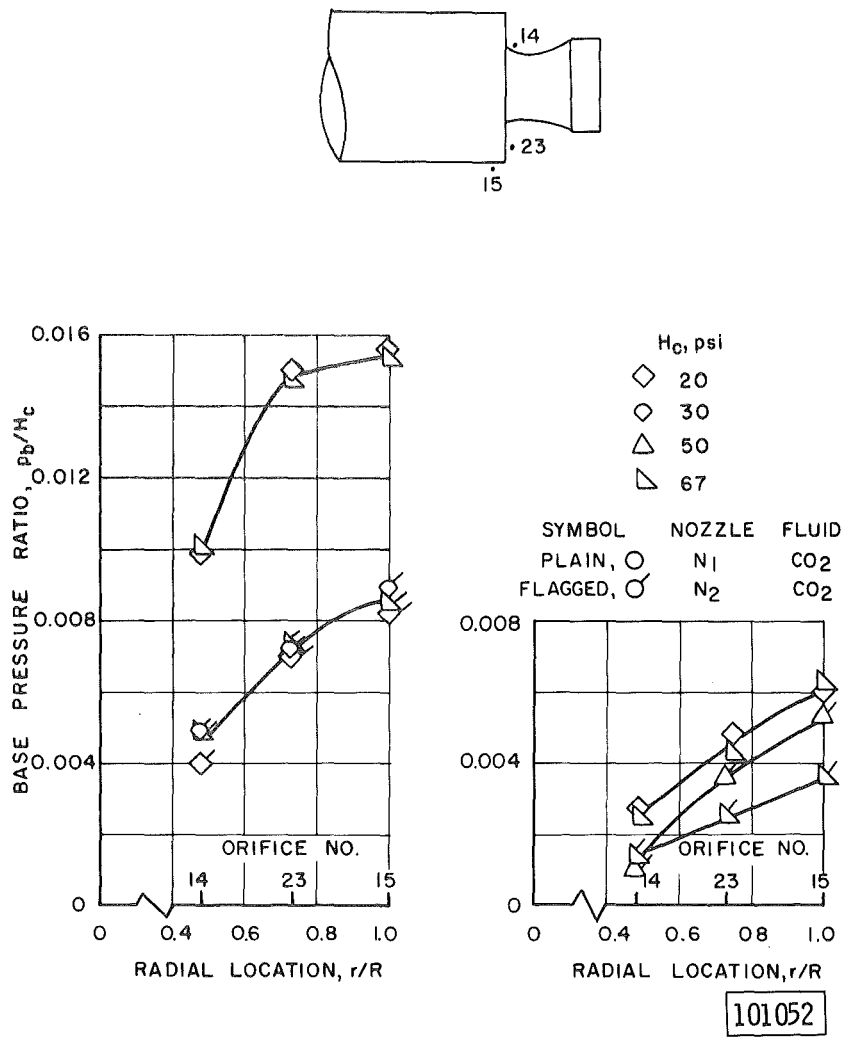

e. x/d = 1.50

f. x/d = 2.00

Fig. 12 Concluded

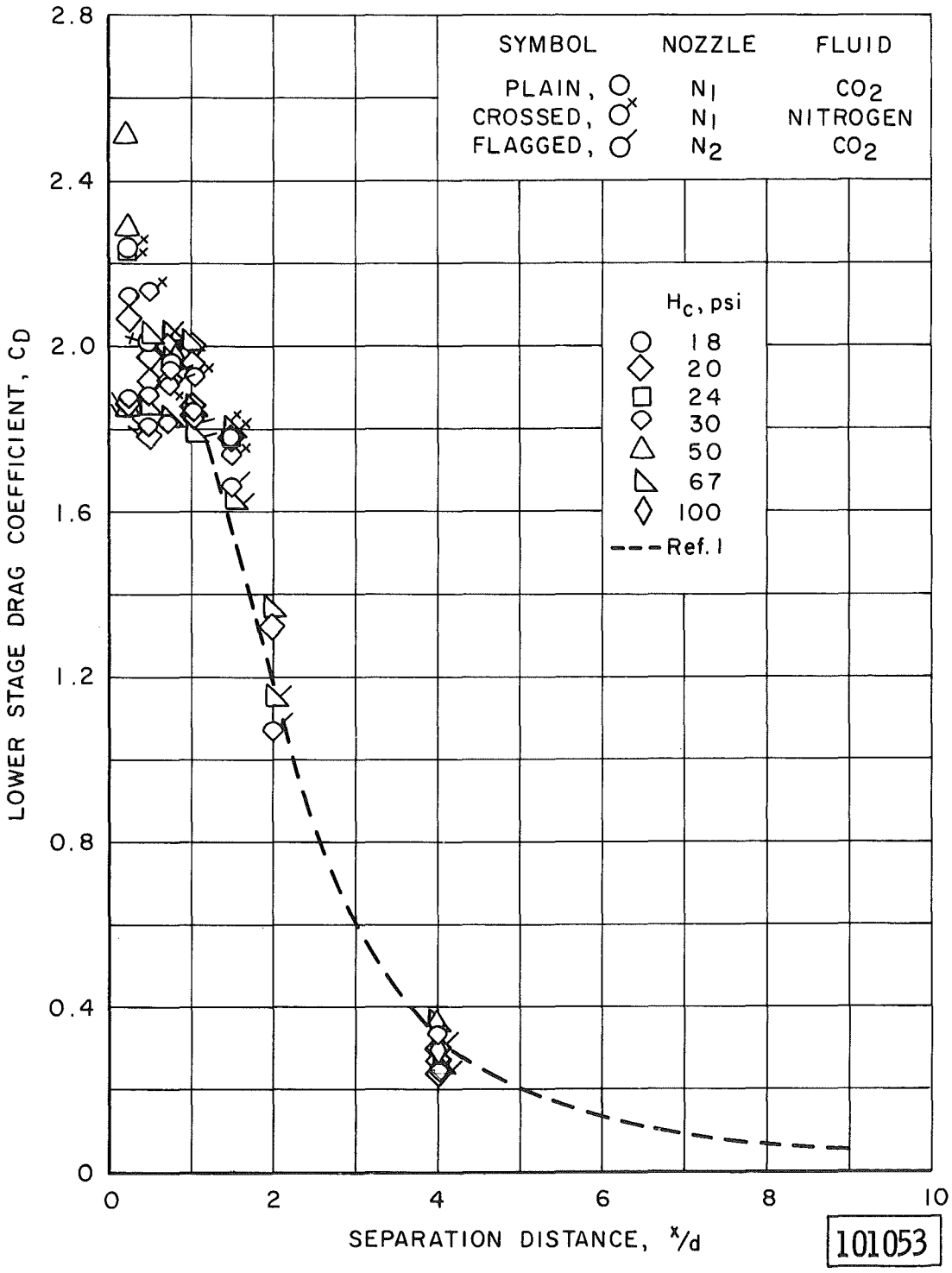

a. C_2 Configuration

Fig. 13 Effect of Separation Distance and Upper Stage Configuration on Lower Stage Drag

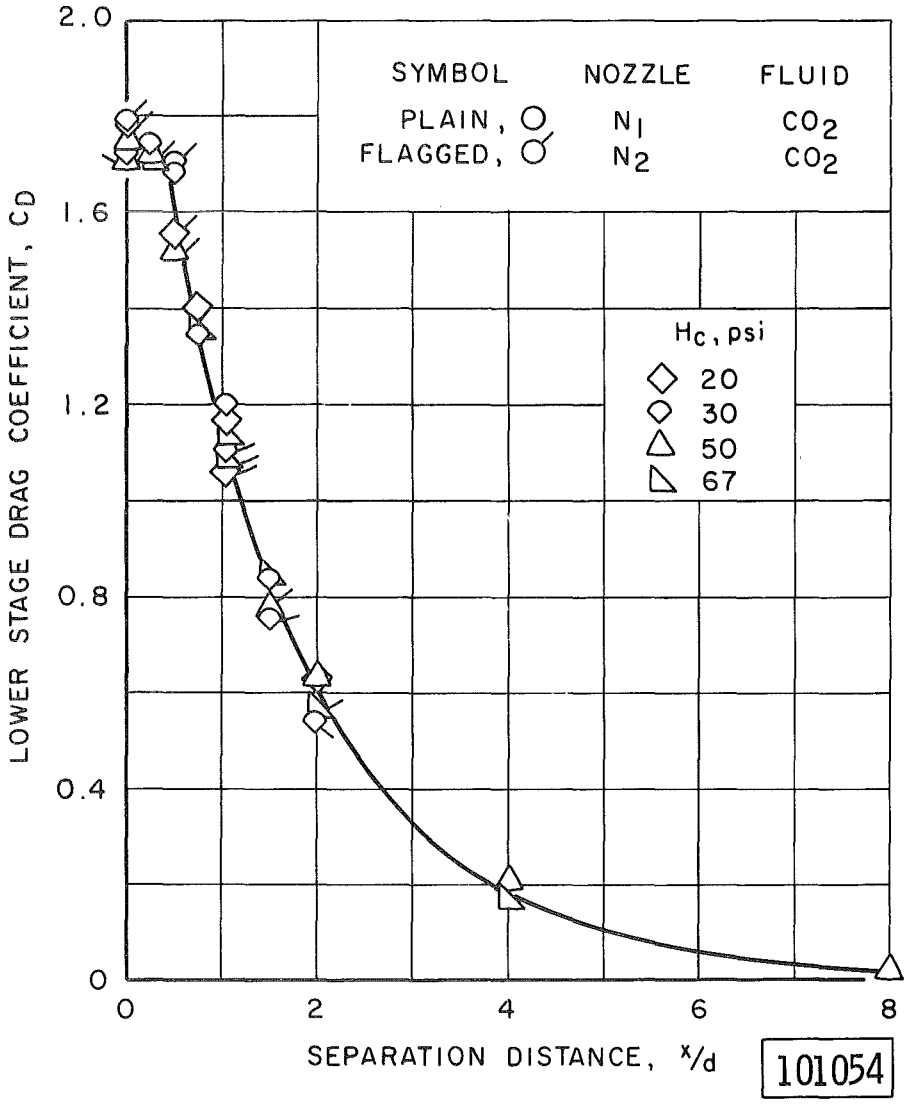

b. C_{2a} Configuration

Fig. 13 Continued

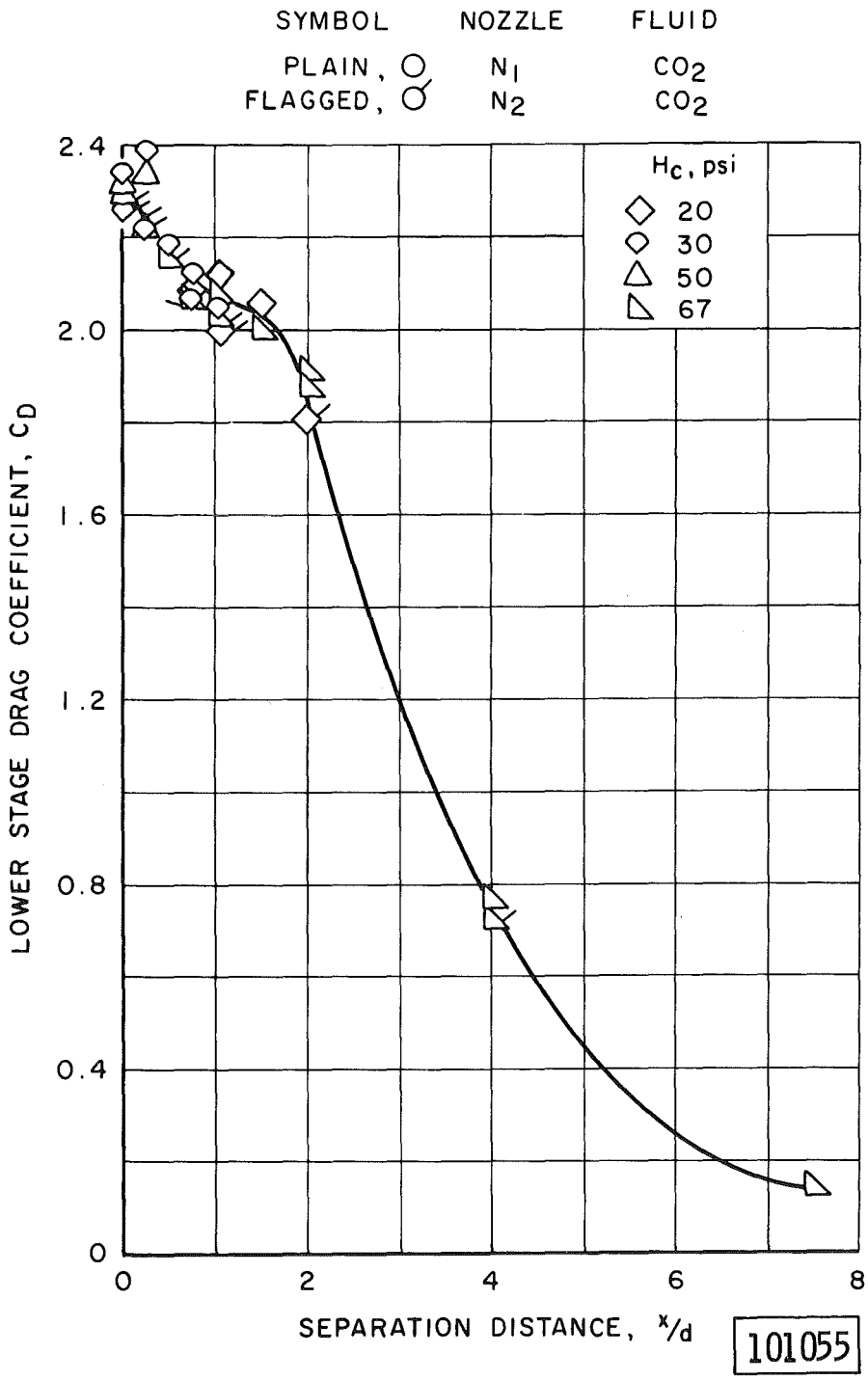

c. C_3 Configuration

Fig. 13 Concluded

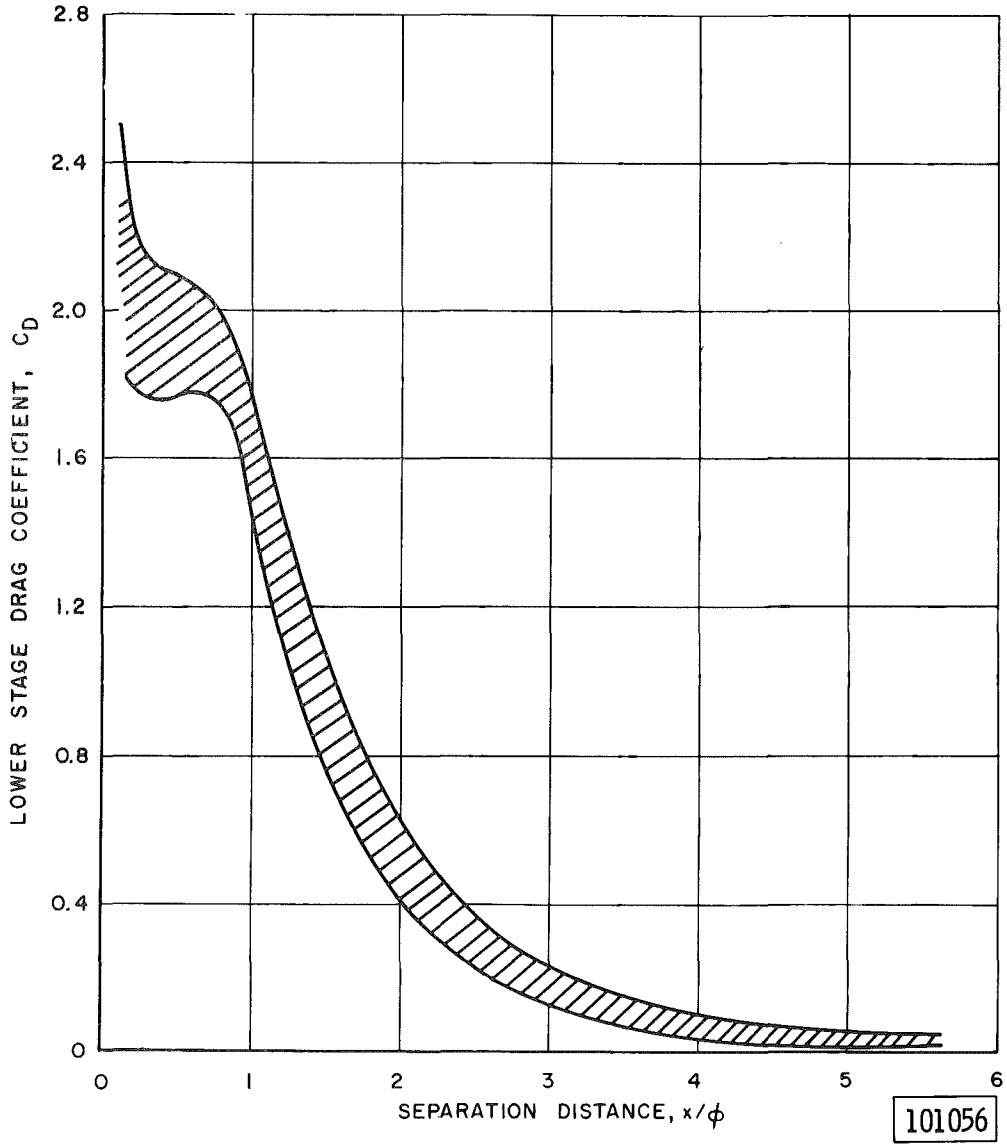

Fig. 14 Generalized Lower Stage Drag

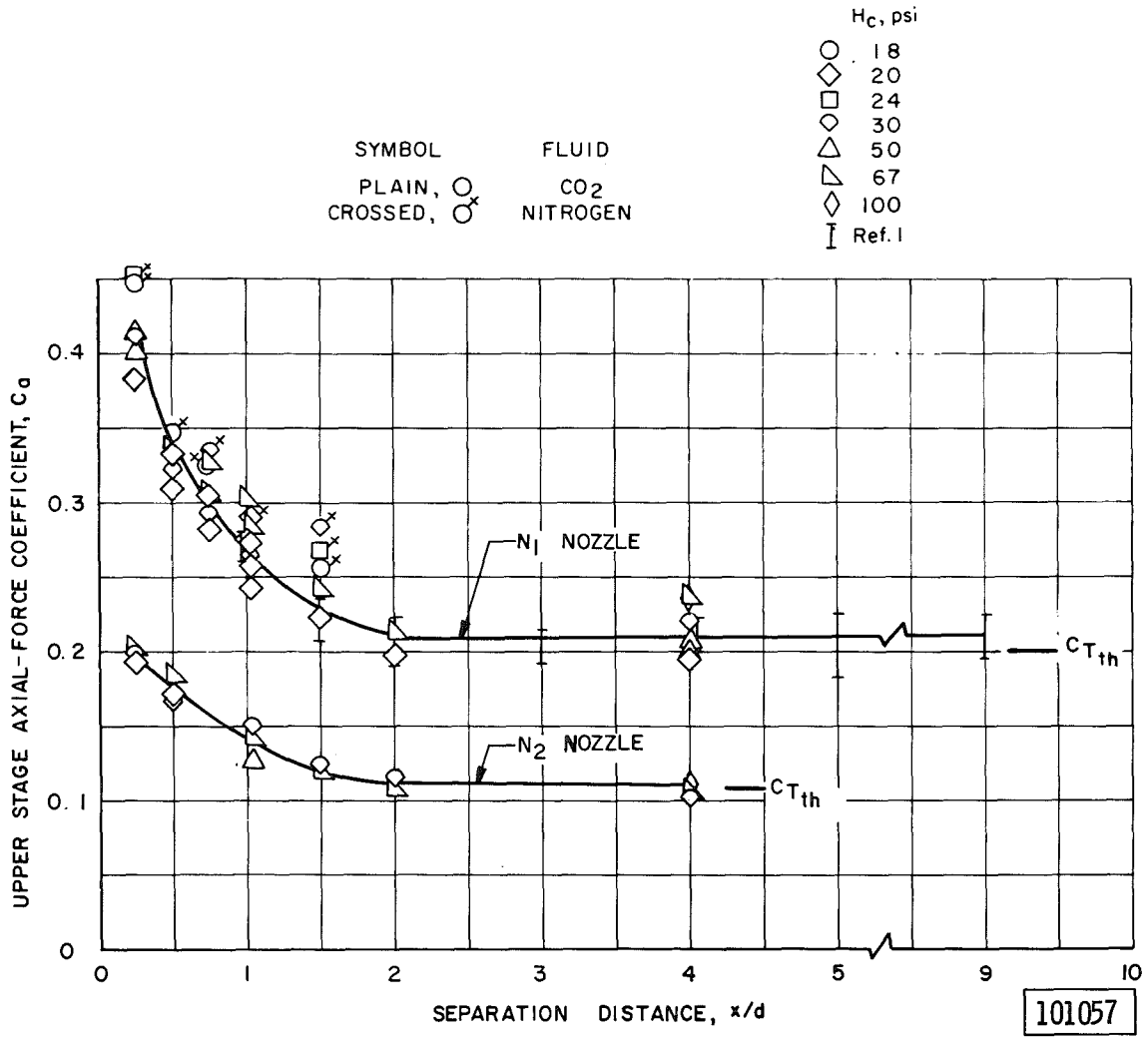

a. C_2 Configuration

Fig. 15 Effect of Separation Distance on Upper Stage Axial-Force Coefficient

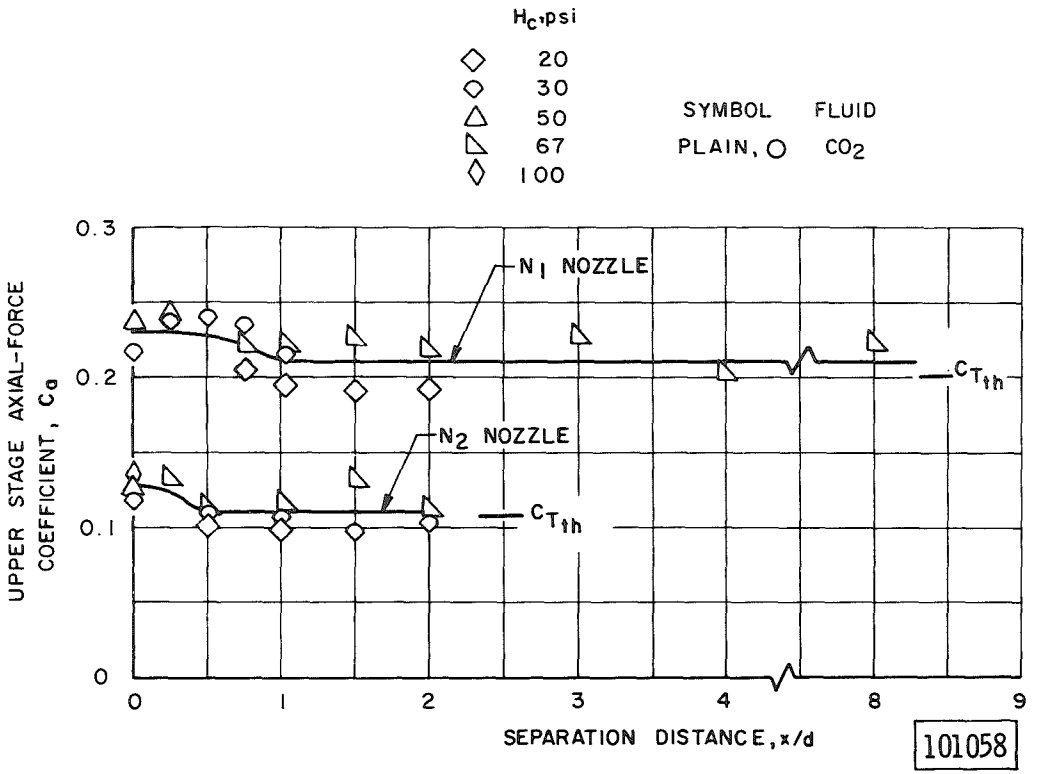

b. C_{2a} Configuration

Fig. 15 Continued

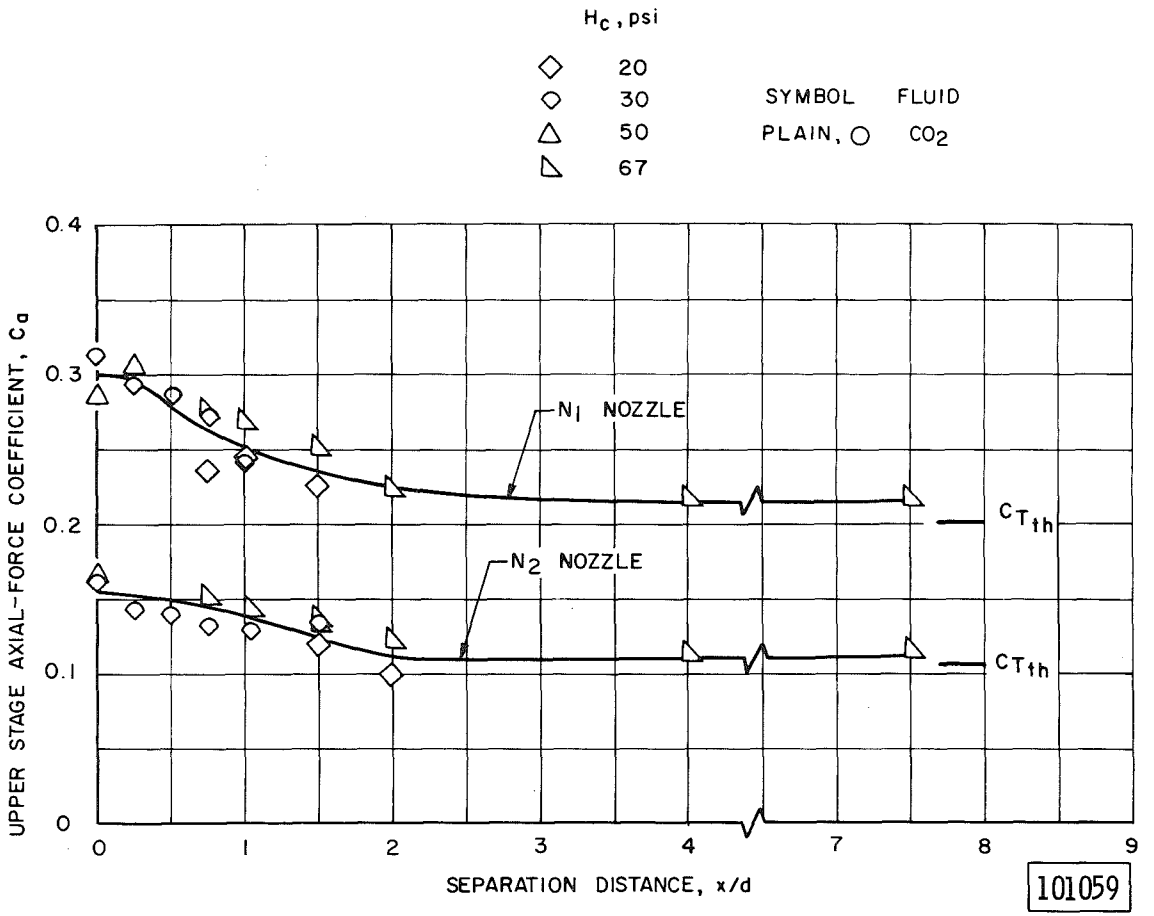

c. C_3 Configuration

Fig. 15 Concluded

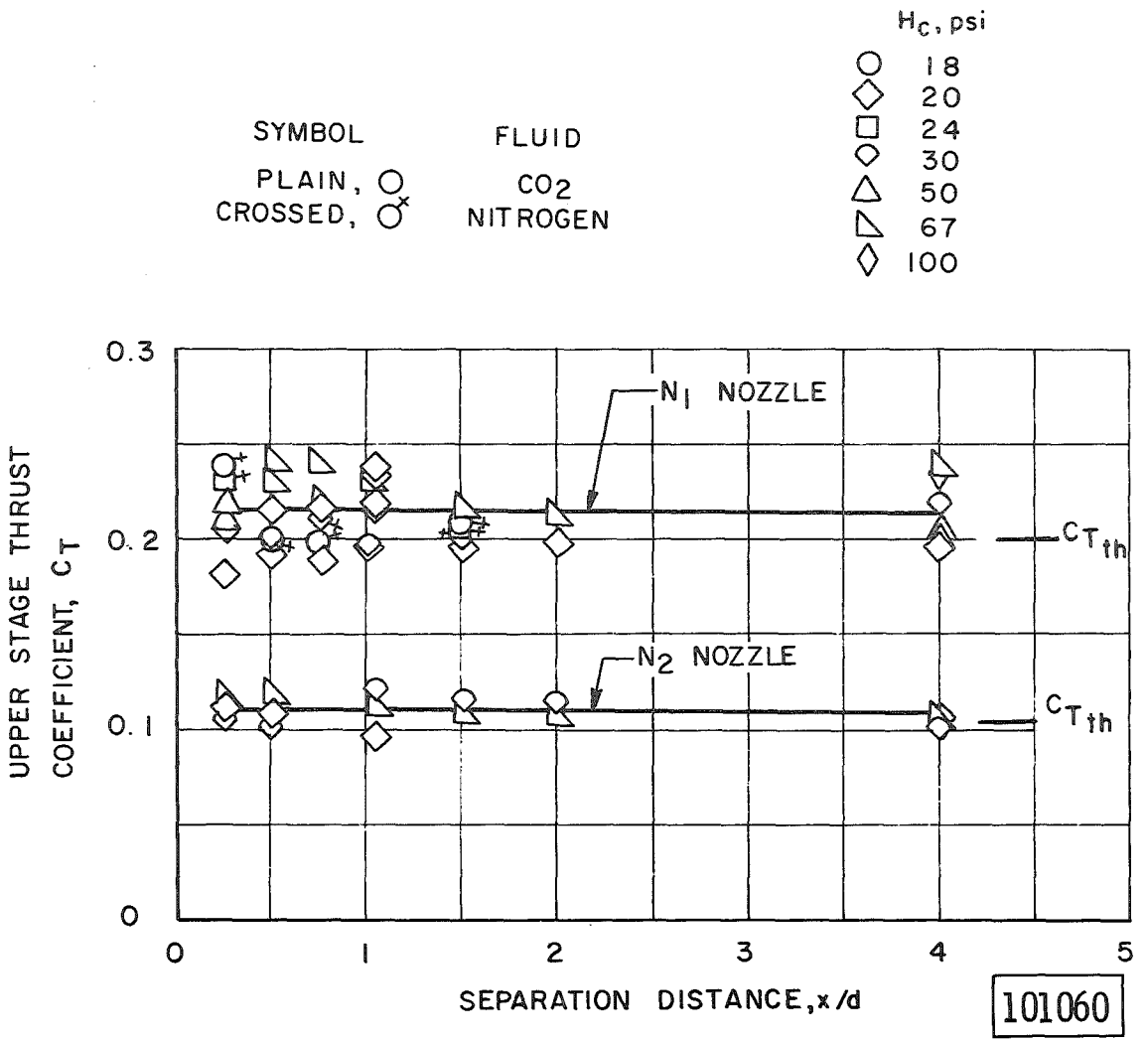

a. C_2 Configuration

Fig. 16 Upper Stage Thrust Coefficient with Each Lower Stage Configuration

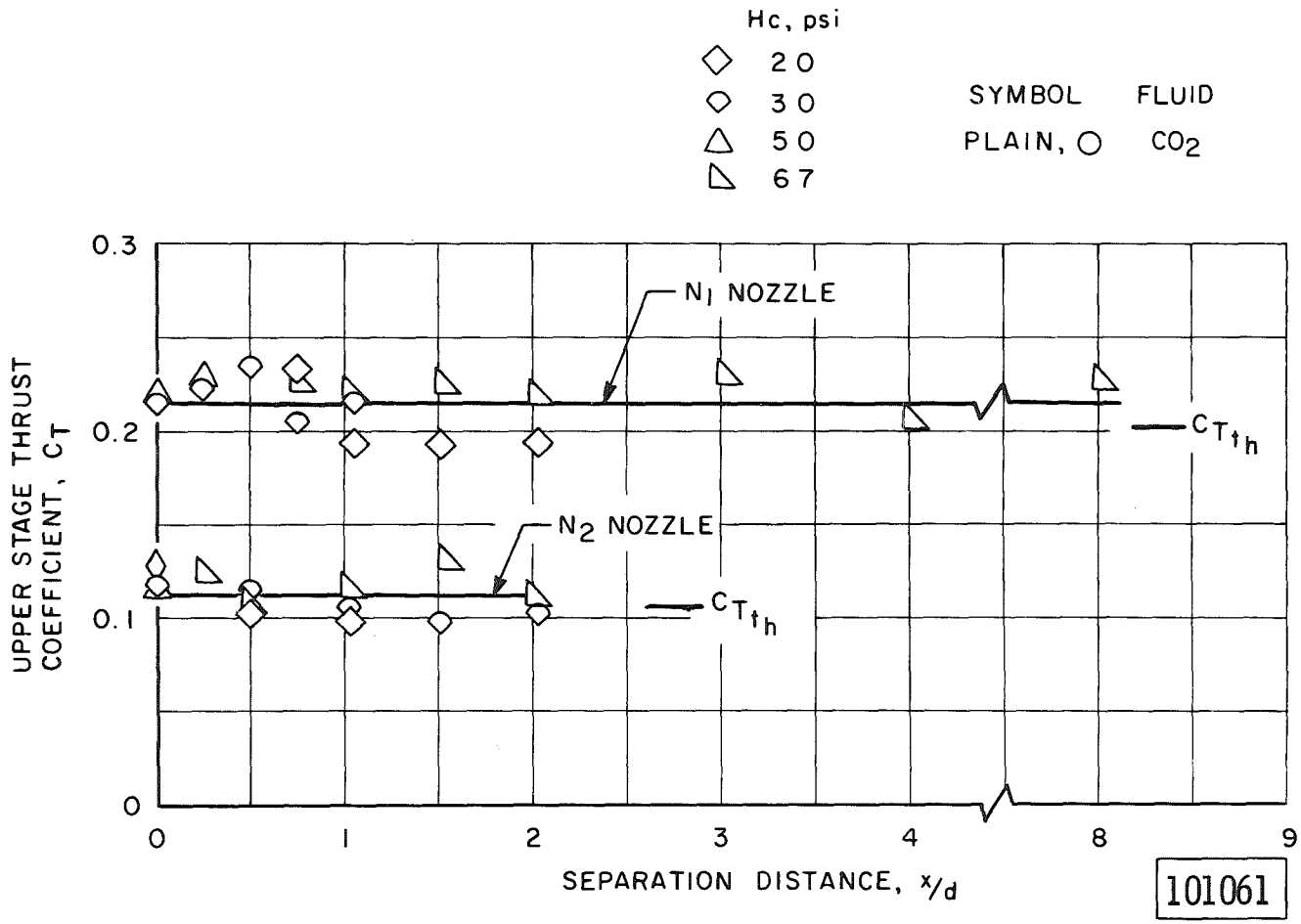

b. C_{2a} Configuration

Fig. 16 Continued

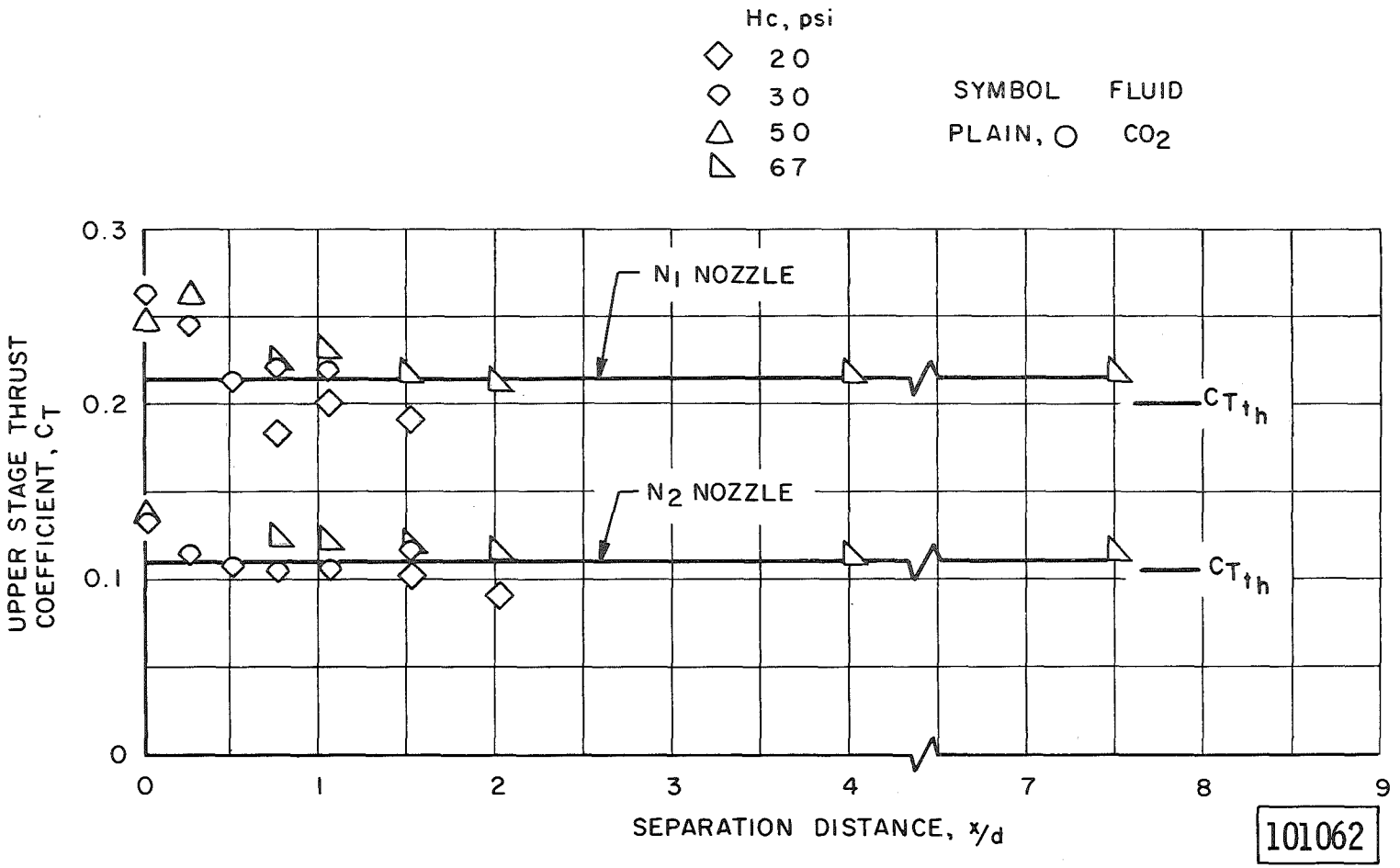

c. C_3 Configuration

Fig. 16 Concluded

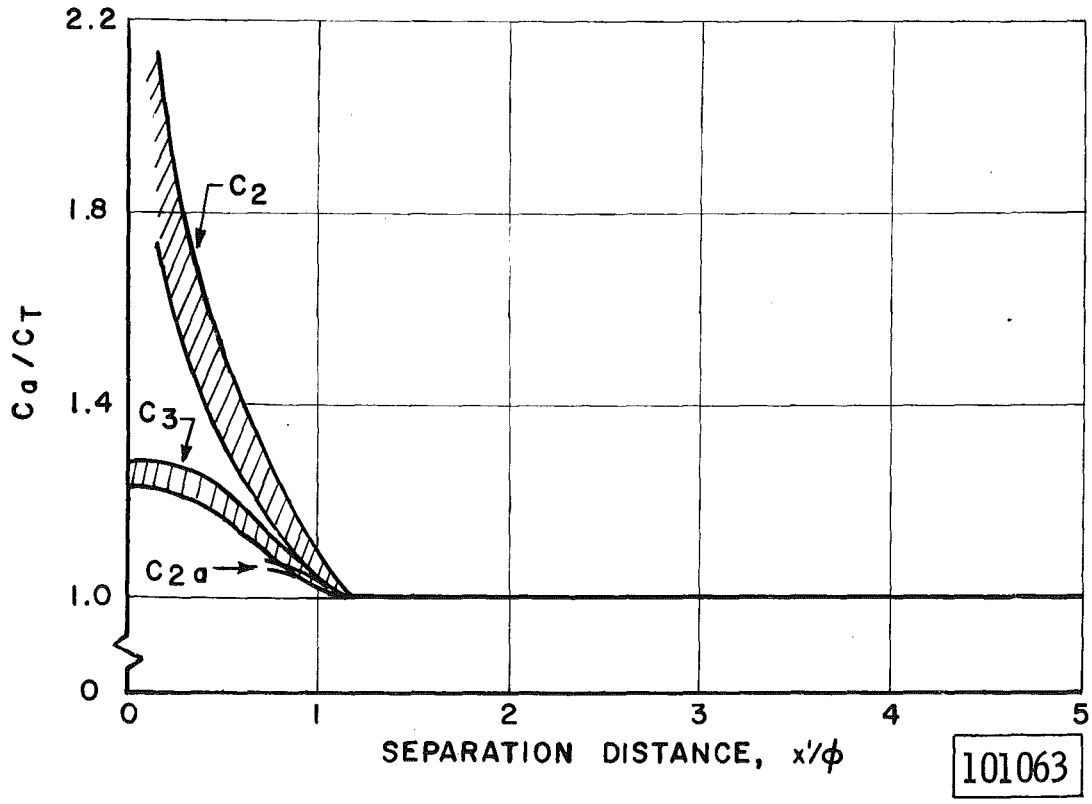

Fig. 17 Effect of Separation Distance on Axial-Force to Thrust Ratio